Mechanical Stimulation Shapes the Immunoregulatory Properties of Dendritic Cells

Zahraa Alraies[1], Claudia A. Rivera[1], Maria-Graciela Delgado[1*], Doriane Sanséau[1*], Matthieu Maurin[1], Aline Yatim[1], Pablo Saez[2 3], Alice Williart[2], Matthieu Gratia[1], Nilushi S. De Silva[1], Aurélie Moreau[4], Benoit Albaud[1], Patricia Legoix[1], Hideki Nakano[5], Donald N Cook[5], Toby Lawrence[6,7], Nicolas Manel[1], Hélène D. Moreau[1], Guilherme P.F. Nader[2#], Matthieu Piel [2#]†and Ana-Maria Lennon-Duménil [1#]†

[1] Institut Curie, PSL University, Inserm U932, Immunity and Cancer, 75005 Paris, France

[2] Institut Curie, PSL Research University, CNRS UMR144; Paris, France

[3] Cell Communication and Migration Laboratory, Institute of Biochemistry and Molecular Cell Biology, Center for Experimental Medicine, University Medical Center Hamburg-Eppendorf, Hamburg, Germany

[4] INSERM, Nantes Université, CHU Nantes, Nantes Université, Centre de Recherche Translationnelle en Transplantation et Immunologie UMR1064, ITUN, Nantes, France

[5] Immunity, Inflammation, and Disease Laboratory, National Institute of Environmental Health Sciences (NIEHS), National Institutes of Health (NIH), Research Triangle Park, North Carolina, USA

[6] Centre d'Immunologie de Marseille-Luminy, Université Aix-Marseille, INSERM, CNRS, Marseille, France

[7] Centre for Inflammation Biology and Cancer Immunology, School of Immunology and Microbial Sciences, King's College London, UK

* These authors contributed equally to the experimental part of this work

# These authors jointly supervised this work

†Corresponding authors: ana-maria.lennon@curie.fr & matthieu.piel@curie.fr

Keywords: immune cells, dendritic cells, cell migration, immune regulation, CCR7, $cPLA_2$, Lamin A/C, ARP2/3, Arpin, F-actin, nuclear ruler pathway, lymph node migration, transcriptional reprogramming, tolerance, immunity.

Abstract

Dendritic cells (DCs) patrol tissues and present collected antigens to T cells in lymph nodes. Migration to lymph nodes requires upregulation of the chemokine receptor CCR7 and allows maintenance of tolerance to self. The signals that trigger CCR7 expression in the absence of infection or inflammation remain unidentified. Here, we show that mechanical stimulation is sufficient to upregulate CCR7 in DCs. This response requires activation of cytosolic phospholipase 2 by nucleus deformation events commonly observed in patrolling DCs. We found that CCR7 upregulation is part of a mechanosensitive transcriptional program that endows DCs with an immunoregulatory phenotype distinct from the one triggered by microbes. Thus, nucleus deformation imprints DCs with chemotactic and immunoregulatory properties compatible with the tolerogenic function previously proposed for these cells.

Introduction

The success of immune responses relies on the ability of immune cells to be at the right time at the right place. These cells circulate between peripheral tissues and lymphoid organs through blood or lymph vessels. Among lymphoid organs, lymph nodes are of major importance as this is where adaptive immune responses are initiated by dendritic cells (DCs) that transport antigens from peripheral tissues to present them to circulating T lymphocytes (1; 2; 3). DC migration and antigen presentation are essential to develop adaptive immune responses against invaders (2; 4; 5). DC migration to lymph nodes also occurs in the absence of infection and inflammation (steady state), a process referred to as homeostatic DC migration, which is needed for presentation of self-antigens and maintenance of tolerance (6). Of note, disruption of homeostatic DC migration has been shown to lead to autoimmunity (6).

To reach and enter lymph nodes, immune cells must upregulate the C-C chemokine receptor type 7 (CCR7) at their surface, which guides them along gradients of CCL21 or CCL19 chemokines (7) (8). The environmental signals that control the expression of CCR7 in immune cells have therefore been intensively investigated. This led to the identification of different molecules such as Pathogen- and Danger-associated Molecular Patterns (PAMPs and DAMPs) (9; 10; 11; 12), in addition to several cytokines and inflammation mediators as potent inducers of CCR7 expression (13; 14; 15). However, even though DCs have been discovered more than 20 years ago, the endogenous signals that induce CCR7 to trigger their homeostatic migration to lymph nodes remain unknown.

So far, these investigations have exclusively focused on chemical signals. Nevertheless, immune cells such as patrolling DCs that display elevated spontaneous motility even in their immature state (16; 17), are also exposed to physical signals. These signals can be mediated by local interactions of the cells with their environment through specific adhesion (18), or result from global deformations of their

cell body and internal organelles (19). Remarkably, we and others have shown that DCs experience and adapt to very large deformations that affect their rigid nucleus when spontaneously migrating through peripheral tissues or dense tumors (20; 21; 22; 23). Such deformations can activate the lipid metabolism enzyme cytosolic phospholipase 2 ($cPLA_2$) (24; 25).This enzyme uses lipids from the nuclear membrane to produce arachidonic acid (AA) that can be converted into Lysophosphatidic acid (LPA), Prostaglandins (PGs) and Leukotriens (LTs) (26; 27; 28; 29), which can exert specific effects on tissue inflammation and thus on local immune responses. Activation of $cPLA_2$ further increases actomyosin contractility of cells undergoing nuclear deformation, allowing them to increase their motility and progress through dense tissues (24; 30). Whether this "nuclear ruler" pathway has any additional impact on gene expression and on the function of immune cells has not been addressed.

In this study, we show that expression of CCR7 in DCs is mechanosensitive: it is triggered upon levels of nuclear deformation that fall within the range of deformations measured in tissue-patrolling DCs (21; 23). Such mechanical stimulation leads to $cPLA_2$-dependent transcriptional reprogramming, endowing DCs with specific immunoregulatory properties distinct from the ones triggered by PAMPS and compatible with their tolerogenic function. We proposed that self-imposed nuclear 'massaging' of tissue patrolling DCs act as an endogenous signal for their homeostatic migration to lymph nodes.

Results

CCR7 expression is induced upon mechanical deformation of DCs

We aimed at evaluating whether the physical deformation of immune cells impacts on their capacity to express CCR7 and might thereby control their ability to home to lymph nodes and build adaptive immune responses. To address this question, we applied precise degrees of deformation on these cells using the confiner device illustrated in figure 1a (31; 32). As immune cell model, we chose unstimulated bone-marrow-derived DCs that express low levels of CCR7 at their surface (33; 34) as often observed in DC populations that reside in peripheral tissues (11). We took advantage of a mouse model harboring a CCR7/GFP reporter gene (35) to evaluate by live imaging the expression dynamics of this chemokine receptor upon DC deformation. CCR7/GFP immature DCs were confined at the heights of 3 and 4μm, which induce distinct degrees of nucleus deformation (fig. 1b), the "nuclear ruler" pathway being turned on only at 3μm-height (24). Importantly, we have previously shown that these confinement heights fall in the 2-4 μm range of deformation measured for the nucleus of DCs that patrol the mouse skin (23) . Fluorescence quantification (supplementary fig. S1a) showed that while GFP expression increased in immature DCs confined at 3 μm height for 4-6 hours, it was not significantly modified in cells confined at 4 μm-height (fig. 1c, d and supplementary movie 1). This was also observed when analyzing the endogenous protein and gene levels of *Ccr7* expression by immunofluorescence and real time quantitative RT-PCR analyses: only immature DCs confined at 3 μm

exhibited a significant increase in CCR7 expression (fig. 1e, f). Of note, the specificity of the anti-CCR7 antibody was verified using *Ccr7*$^{GFP/GFP}$ DCs (supplementary fig. S2b). A similar observation was made when cells were confined for 30 minutes, harvested and *Ccr7* was checked by after RT-PCR 4 hours (fig. 1g). These results suggest that imposing a 30 minute-deformation at 3µm-height on the nucleus of immature DCs is sufficient to upregulate CCR7 expression.

Importantly, CCR7 expressed at the surface of DCs confined at 3 µm height was fully functional, as addition of its ligand CCL19 at one side of the confinement device triggered chemotaxis (fig. 1h). A significantly smaller response was observed when DCs were confined at 4 µm-height, consistent with the lack of CCR7 surface expression in this experimental condition. Accordingly, in these confinement condition, cells confined at 3 µm height exhibited faster migration speed than the cells confined at 4-µm height close to CCL19 chemokine gradient (fig. 1h). We conclude that deformation of immature DCs at 3µm-height leads to up-regulation of CCR7 expression, endowing DCs with the ability to perform chemotaxis along CCL19 gradients.

Mechanical upregulation of CCR7 expression depends on the lipid metabolism enzyme cPLA$_2$

We next asked whether CCR7 up-regulation in DCs deformed at 3µm height required activation of the "nuclear ruler" pathway. For this, we either treated immature DCs with the AACOF3 cPLA$_2$ inhibitor or knocked down cPLA$_2$ using siRNA (supplementary fig. S2a). We found that both cPLA$_2$ inhibition and knock down abrogated the upregulation of CCR7/GFP expression induced by cell deformation at 3 µm-height (fig. 2a, b). In sharp contrast, cPLA$_2$ inhibition or knock down did not prevent the upregulation of CCR7 expression in response to treatment with the microbial compound lipopolysaccharides LPS (supplementary fig. S2b, c). These results indicate that this lipid metabolism enzyme is specifically required for CCR7 expression induced by cell deformation, rather than generally involved in the transcriptional regulation of the *Ccr7* gene. Hence, the induction of CCR7 by mechanical stimulation requires cPLA$_2$.

In zebrafish neutrophils and mammalian epithelial cell lines, cPLA$_2$ activation in response to nuclear stretching is thought to result from an increase in nuclear envelope tension (25; 36; 37). Consistent with these findings, we observed that nuclear envelop fluctuations diminished when confining DCs at 3 µm-height (supplementary fig. S2d), suggesting a tension increase (38; 39). On the same line, DCs knock out for Lamin (Lmn) A/C, a nucleoskeleton protein needed for cells to build up nuclear envelop tension upon confinement (40; 41), did not upregulate CCR7 when confined at 3 µm-height (fig. 2c). In addition, we found that confinement at 2 µm-height, which triggers nuclear envelop ruptures (fig. 2d and supplementary movie 2) and loss of Lamin A/C (fig. 2h) and should thus not lead to a sustained high envelop tension, did not induce *Ccr7* upregulation in immature DCs (fig. 2e). This was not due to increased cell death, which exhibited low rates at the three confinement heights (< 8% of death in all

confinement conditions). DCs confined at 2 µm-height did not display any sign of damage since they were able to upregulate *Ccr7* expression upon LPS treatment (supplementary fig. S2e). These results argue in favor of CCR7 expression being upregulated downstream of $cPLA_2$ activation upon an increase in nuclear envelop tension, and thus being under the control of the "nuclear ruler" pathway. Consistently, quantification of $cPLA_2$ subcellular localization revealed that the enzyme was accumulated in the nucleus of DCs confined at 3 µm-height, and not at 4 or 2 µm (fig. 2f), and $cPLA_2$ nuclear translocation was not observed in Lmn A/C^{KO} DCs confined at 3 µm-height (fig. 2g). Of note, despite the extensive deformation experienced by the nuclei of DCs confined at 2 µm-height, $cPLA_2$ does not accumulate into their nucleus, ruling out any imaging artifact due to nuclear shape and strongly arguing for nuclear envelope stretching, rather than mere nucleus deformation, being responsible for the activation of this lipid metabolism enzyme. We conclude that deformation of the nucleus of immature DCs leads to enhanced nuclear membrane tension and subsequent $cPLA_2$ activation, which in turn allows the upregulation of CCR7 expression.

Activation of $cPLA_2$ and induction of CCR7 expression are tuned by the ARP2/3 complex

Lmn A/C is part of the LINC complex that connects the nucleoskeleton to the actin cortical cytoskeleton (42; 43; 44). Such connection is needed for the actin cytoskeleton to exert mechanical forces on the nucleus and might contribute to increase nuclear envelop tension. Distinct actin pools have been described to assemble in the perinuclear area of cells undergoing physical deformation (45; 21), including in immature DCs, where a perinuclear cage of branched actin is nucleated by the ARP2/3 complex in response to confinement (21). We therefore investigated whether ARP2/3 was needed for induction of CCR7 expression by nucleus confinement. Treatment of immature DCs with the ARP2/3 inhibitor CK666 impaired the upregulation of *Ccr7* expression upon confinement at 3 µm-height (fig. 3a). The nuclear accumulation of $cPLA_2$ was also compromised in CK666-treated immature DCs confined at 3 µm-height (fig. 3b), showing that the activation of the lipid metabolism enzyme relies on ARP2/3-dependent nucleation of branched actin.

To strengthen this result, we investigated the response to nuclear deformation of DCs knock out for the ARP2/3 inhibitor (*Arpin* $^{flox/flox}$ x CD11c-CRE) (46). Remarkably, we found that $Arpin^{KO}$ immature DCs underwent a shift in their sensitivity to nuclear deformation as they upregulated *Ccr7* when confined at 4 instead of 3 µm-height (fig. 3c). $Arpin^{KO}$ immature DCs confined at 4 µm-height accumulated $cPLA_2$ in their nucleus almost to the same extent observed in DCs from $Arpin^{WT}$ DCs confined at 3 µm-height, suggesting that it is activated in $Arpin^{KO}$ cells already at the height of 4 µm (fig. 3d). Of note, induction of *Ccr7* expression in $Arpin^{KO}$ DCs was $cPLA_2$-dependent, as observed in wild-type cells (fig. 3e). Live-imaging revealed that, when confined at 4 µm-height, $Arpin^{KO}$ DCs exhibited a cloud of perinuclear F-actin that was not observed in their wild-type counterpart under the same height but observed in wild-

type cells confined at 3 µm (fig. 3f, supplementary movie 3). These data show that the activity of ARP2/3 determines the sensitivity of immature DCs to nuclear deformation, defining a threshold for $cPLA_2$ activation and induction of CCR7 expression in response to physical confinement.

Interestingly, the WASP nucleation promoting factor (NPF) has recently been shown to activate ARP2/3 in the perinuclear area of DCs (47). We therefore investigated whether this NPF was required for the response of immature DCs to nucleus deformation. We found that $WASP^{KO}$ DCs did not upregulate CCR7 surface expression upon confinement at 3 µm-height (fig. 3g), a phenotype that resembled the one of CK666-treated DCs. Altogether, these results show that branched F-actin nucleated by ARP2/3 tunes the capacity of DCs to activate the nuclear ruler pathway and upregulate CCR7 expression in response to confinement-induced nuclear deformation.

Increased homeostatic migration to lymph nodes of skin DCs exhibiting elevated ARP2/3 activity

CCR7 up-regulation in DCs triggers their migration to lymph nodes. By restraining $cPLA_2$ activation and downstream induction of CCR7 expression in response to nucleus deformation, Arpin might therefore act as a negative regulator of homeostatic DC migration to lymph nodes. This process could limit the number of DCs that become CCR7-positive upon the nuclear deformation events they experience while patrolling peripheral tissues (43; 21). To test this hypothesis, we assessed by flow cytometry whether Arpin deficiency altered the number of migratory DCs present in skin-draining lymph nodes at steady state, i.e. in the absence of any external stimulation. This experiment showed that the number of $Arpin^{KO}$ migratory DCs found in lymph nodes was increased, as compared to wild-type migratory DCs (fig. 4a, b). This particularly concerned the main subtype of conventional DCs (cDCs) that migrate to lymph nodes in homeostasis, migratory cDC2s. No such difference was observed when quantifying lymph node-resident DCs. Analysis of DC numbers in the skin showed a slight, although not statistically significant, decreased number of $Arpin^{KO}$ cDC2s (fig.4c, d). This result excludes the possibility that increased numbers of migratory cDC2s in lymph nodes result from increased presence of cDC2s in the skin of $Arpin^{KO}$ mice. Altogether, these data are consistent with $Arpin^{KO}$ cDC2s leaving the skin at higher frequency as compared to wild-type cells, leading to increased numbers of cDC2s in lymph nodes at steady-state.

ARP2/3 deficiency has been shown to regulate immune cell migration and chemotaxis *ex vivo* and *in vivo* (48; 49; 50; 51). We therefore assessed whether $Arpin^{KO}$ DCs displayed enhanced chemotactic migration along CCL19 gradients in collagen gels, as this could also account for their increased migration to lymph nodes at steady state. Noticeably, no difference was observed in the ability of LPS-treated DCs to express surface CCR7 and follow CCL19 gradients, they even displayed slower migration phenotype as compared to their WT counterparts (fig. 4e, f). Altogether, these results suggest that the levels of ARP2/3 activity tune the number of DCs that migrate to lymph nodes at steady state by

controlling $cPLA_2$ activation and downstream CCR7 expression in response to nucleus deformation. They further suggest that DC homeostatic migration can result from their mechanical stimulation.

$cPLA_2$ controls a mechanosensitive transcriptional program regulating homeostatic DC migration

Activation of $cPLA_2$ has been associated to transcriptional changes in different cell types (52; 53; 54; 55). We thus asked whether induction of CCR7 expression was part of a global transcriptional program triggered upon nucleus deformation. Indeed, such program could shape the immunoregulatory properties of the DCs that migrate to lymph nodes upon activation of the nuclear ruler pathway at steady state, thereby impacting on the type of T cell response they induce. To address this question, we analyzed by bulk RNAseq the transcriptome of DCs expressing or not $cPLA_2$ (*Pla2g4a*) and confined at 3 µm-height, non-confined cells were used as negative controls. The overview of the gene expression profiles obtained showed that, while non-confined wild-type and $cPLA_2$ KO cells seemed very similar, confined $cPLA_2$ KO cells had lost a large proportion of the genes induced by nuclear deformation in their wild-type counterpart (fig. 5a). Principal component analysis provided a clear quantitative assessment of this effect: while non-confined wild-type and $cPLA_2$ KO samples clustered together with similar PC1 and PC2 values, confined cells showed very different values in WT and $cPLA_2$ KO DCs (fig. 5b). Focusing on the genes that significantly varied (p-value <= 0.05 and fold-change >= 1.5) between confined and non-confined conditions, we observed that ~2000 and ~1800 genes were up and downregulated in immature wild-type DCs confined at 3 µm-height, respectively (fig. 5c, see red and yellow ellipses). Comparison of $cPLA_2$-sufficient (*$Pla_2g4a^{flox/flox}$* CD11c-CRE-/-) and -deficient (*$Pla_2g4a^{flox/flox}$* CD11c-CRE+/-) DCs showed that a large fraction (about half) of the genes that were up- or downregulated by nuclear deformation in wild-type cells were not significantly changed in $cPLA_2$ KO DCs (fig. 5c, see blue and green ellipses). Pathway analysis revealed that the genes whose upregulation was lost in $cPLA_2$ KO DCs were enriched for distinct innate immunity-related (cytokines, interferon, interleukins, and NFκB activation) as well as antigen processing pathways (fig. 5d). Altogether, these results suggest that nucleus deformation leads to a transcriptional reprogramming of DCs and modulates genes related to their immunomodulatory properties in manner that mostly depends on $cPLA_2$.

In agreement with our findings above, we observed that *Ccr7* upregulation was fully lost in cells lacking $cPLA_2$, which even rather showed a decrease in *Ccr7* levels upon confinement (fig. 5e – note that since *Ccr7* was almost not expressed in non-confined DCs, this further reduction might not have a strong functional meaning). Among the genes following the same expression pattern (not expressed in non-confined DCs and induced by confinement in wild-type but not in $cPLA_2$ KO DCs) were two genes associated with ARP2/3-dependent actin nucleation as well as the *Ikbkb* gene (fig. 6a). The latter was of particular interest as this NFκB-activating kinase has been shown to control the homing of skin

cDC2s to lymph nodes at steady state (6), in line with our data suggesting that $cPLA_2$ also plays a role in this process. We therefore investigated whether $cPLA_2$ (*Pla2g4a*) and Ikkβ (*Ikbkb*) could be part of the same signaling pathway. We found that confinement did not induce *Ccr7* upregulation in cells treated with the Ikkβ inhibitor BI605906 and in *Ikbkb* knock out DCs (fig. 6b, c). Furthermore, while NFκB nuclear translocation was compromised in cells lacking $cPLA_2$, Ikkβ inhibition did not affect the nuclear accumulation of $cPLA_2$ in confined cells (fig. 6d, e). These findings suggest that Ikkβ induction and NFκB nuclear translocation are downstream of $cPLA_2$ activation in confined cells. Of note, several genes associated to the type I interferon (IFN) response, including several IFN related genes and IFN-sensitive genes (ISGs), also followed the same expression pattern than *Ccr7* and Ikkβ *(*fig. 6f). This result is in agreement with previous findings highlighting that cDC2s migrating from the skin to lymph nodes at steady state exhibited a type I IFN signature (56), in addition to their NFκB one (6). Our findings are consistent with a model when deformation of the nucleus of DCs leads to Arp2/3-dependent activation of $cPLA_2$, which induces Ikkβ and NFκB nuclear translocation. This leads to transcriptional changes that (1) upregulate *Ccr7* expression, promoting the homeostatic migration to lymph nodes of DCs and (2) endows these cells with the capacity to harbor a specific immunoregulatory phenotype.

Mechanical stimulation specifically shapes the immunomodulatory properties of DCs

Beyond type I IFN, we found that distinct genes linked to innate sensing pathways were upregulated in a $cPLA_2$-dependent manner in DCs confined at 3 µm-height (fig. 6g). To assess whether this was specific of mechanically stimulated DCs or more generally applied to activated DCs, we evaluated the $cPLA_2$ dependency of the transcriptome of LPS-treated cells. Astonishingly, this experiment showed that $cPLA_2$ had no significant impact on the global gene expression pattern of LPS-treated DCs (fig. 7a and b, see also PCA in fig. 5b and Volcano plots in fig. S3a). In agreement with this result, when comparing the expression of the $cPLA_2$ gene itself (*Pla$_2$g4a*) and several genes related to the $cPLA_2$ pathway, we observed that several were more up-regulated in DCs confined at 3 µm-height as compared to LPS-treated cells (fig. 7c). Among the genes that significantly varied (p-value <= 0.05 and fold-change >= 1.5) between wild-type samples, about 1500 genes were upregulated in both LPS and mechanically stimulated cells (fig. 7b). Importantly, induction of these genes was lost in confined but not in LPS-treated $cPLA_2$ KO DCs, showing that the same large set of genes is controlled by different pathways in response to these two stimuli. Pathway analysis highlighted that the genes specifically upregulated in response to LPS, but not to mechanical stimulation, were mainly associated to the immune response (1221 genes, fig. 7b blue ellipse and fig. 7d). The genes specifically upregulated in response to mechanical stimulation belonged to lipid metabolism and antigen presentation (489

genes, fig. 7b red ellipse and fig. 7e). Of note, although both mechanical and LPS responses led to up-regulation of the NFκB pathway (fig. 7d pathways in orange), the precise genes concerned were distinct (fig. 7f). In particular, we observed that the expression of proteasome (PSM) genes belonging to the NFκB pathway was induced by LPS treatment but not by mechanical confinement. Altogether these results highlight that mechanical deformation of the nucleus of DCs transcriptionally reprograms these immune cells in a way distinct from microbial activation and with a different requirement for $cPLA_2$.

We observed that LPS-activated DCs expressed higher levels of genes encoding for cytokine and co-stimulatory molecules (examples in supplementary fig. S3c). We experimentally confirmed that IL1b, IL12a, IL27, and IL15 were indeed secreted at higher levels in LPS-activated DCs as compared to mechanically stimulated cells (supplementary fig. S4c bottom). In addition, cytometry analysis of CD80, CD86, and MHCII surface expression showed that these co-stimulatory molecules were induced at lower levels in confined DCs, as compared to LPS-activated cells (fig. 7g). These results suggest that mechanically stimulated DCs might be less potent than LPS-treated cells for T lymphocyte activation. To address this question, we loaded the two types of DCs with the ovalbumin (OVA) peptide and incubated them with OT-II transgenic T cells, which specifically recognize these MHC II-peptide complexes. These experiments unambiguously showed that mechanically stimulated DCs were less efficient than LPS-treated cells in T lymphocyte activation, although cell viability was comparable in both conditions (fig. 7h, supplementary fig. S3d). A similar result was obtained performing Mixed Leukocyte Reactions (MLR) (supplementary fig. S3e). These findings confirm that mechanically stimulated DCs are in a distinct activation stage as compared to microbe-activated DCs, displaying a milder T cell activation capacity. They are consistent with the tolerogenic properties that had previously been proposed for DCs migrating to lymph nodes in homeostasis.

Discussion

Here we show that expression of the chemokine receptor CCR7, responsible for migration of immune cells to lymph nodes, can be mechanically triggered by the nuclear ruler pathway, which is under the control of the lipid metabolism enzyme $cPLA_2$. Activation of this phospholipase is induced upon confinement of DCs at a range of deformation similar to what was observed in DCs patrolling peripheral tissues such as the skin (57; 12; 23) or the tumor microenvironment (58). We further highlight that the nuclear ruler pathway is tuned by the ARP2/3 complex, which is responsible for the formation of branched actin networks, and whose level of activity is controlled by its inhibitor Arpin in DCs. Remarkably, we found that this pathway does not only trigger CCR7 expression, but specifically

reprograms the transcription of mechanically stimulated DCs towards an immunoregulatory phenotype distinct from the one they harbor upon activation with PAMPs such as LPS.

We found that the nuclear ruler pathway modulates both the chemotactic and immunomodulatory properties of DCs, suggesting that the events of nucleus deformation that these cells experience while migrating in peripheral tissues might influence their ability to shape T lymphocyte responses once in lymph nodes. Indeed, we found that mechanically stimulated DCs express less pro-inflammatory cytokines as compared to the ones that are typically expressed upon treatment with PAMPs. Furthermore, although mechanically stimulated DCs express co-stimulatory molecules such as CD80 and CD86, their surface levels are decreased as compared to the ones observed in LPS-treated DCs. This is consistent with mechanically stimulated DCs being less efficient in triggering T cell activation and proliferation, and compatible with the tolerogenic function that has been proposed for these cells at steady state. Our findings therefore suggest that nucleus deformation might be a tissue intrinsic physical signal that instructs DCs to home to lymph nodes at steady state. This is consistent with our data showing the requirement of $cPLA_2$ to trigger Ikkβ and NFκB activation, which are known to control homeostatic DC migration to lymph nodes. Of note, more than 20 years after the discovery of DCs, the signal(s) that induce their homing to lymph nodes at steady state remain(s) unknown. Our work supporting the intriguing hypothesis that this signal might be of physical origin potentially explains why it has not been identified so far.

We propose that activation of the nuclear ruler pathway in DCs that undergo successive event of nucleus deformation as they move through peripheral tissues, could gradually imprints them with a tolerogenic properties to ultimately induce CCR7 expression, promoting their migration to lymph nodes. The function of the nuclear ruler pathway in this context could thus be viewed as an internal molecular clock that helps DCs “measuring the time” they have spent patrolling tissues as a function of the number and/or extent of nucleus deformation events they have experienced. This implies that DCs within dense tissues imposing larger physical constrains, such as in the skin, the lungs, fibrotic tissues or tumors, might reduce their time of residency and/or alter their immunoregulatory properties. Interestingly, a recent study has identified a mouse tumor-resident DC population, referred to as “mature reg (mReg) DCs”, which shares similarities with our mechanically stimulated DCs: both populations harbor a mature phenotype, characterized by the presence of CCR7 on their surface, but also express numerous immunoregulatory genes (59). Future studies aimed at analyzing the role of $cPLA_2$ in the emergency of mReg DCs should help evaluating the contribution of the nuclear ruler pathway to anti-tumor immunity.

Our results show that mechanosensitive reprogramming of the DC phenotype requires the nucleoskeleton component Lmn A/C. Interestingly, it was recently highlighted that the production of pro-inflammatory cytokines in response to LPS in macrophages rely on Lmn A/C disassembly (60): LPS-treated cells disassemble Lmn A/C to produce type I IFNs, which then act in an auto- and paracrine manner to stimulate the transcription of cytokine genes (60). This pathway is reminiscent of the one we describe here for mechanically stimulated DCs, in which type I IFNs gene transcription is also induced, but in response to $cPLA_2$ activation and in a Lmn A/C-dependent manner. Thus, the immunoregulatory phenotype of tissue resident DCs would be maintained "by default" via the Lmn A/C-dependent activation of the nuclear ruler pathway, preventing them from migrating to lymph nodes in a pro-inflammatory state in homeostasis. In contrast, upon tissue infection this mechanical activation of DCs would be canceled by PAMP-induced Lmn A/C disassembly, thereby allowing the adaptive immune response to be turned on for elimination of the infectious agent. Such mechanism might be particularly relevant in tissue resident DCs expressing higher levels of Lmn A/C gene, such as the ones residing in the skin and lungs (Web based immgen data) (61), which might thus be more prone to respond to mechanical stimulation by activating the nuclear ruler pathway. Whether DCs express or not Lmn A/C could therefore define the balance between tolerance and immunity depending on the physical properties of tissues. It is worth noting that the skin and lungs are also particularly exposed to microbial components and may therefore require additional protection mechanisms to prevent PAMP-mediated DC activation at steady-state.

In conclusion, we here propose that self-imposed nuclear 'massaging' that DCs experience while patrolling their environment at steady state might promote the emergence of a population of migratory cells that arrive to lymph nodes harboring specific immunomodulatory properties compatible with their tolerogenic function. We foresee that this $cPLA_2$-dependent mechanosensitive pathway might also impact the physiology of other $cPLA_2$-expressing cells, for example monocytes, which rely on CCR7 and on the PGE-producing enzyme COX to home to tissues at steady-state (62), or tumor cells, which use CCR7 to invade healthy tissues by first migrating to lymph nodes (63; 64; 65; 66).

Acknowledgments:

Funding: This project has received funding from the European Union's Horizon 2020 research and innovation program under the Marie Skłodowska-Curie grant agreement No 666003. This work has also received support under the program «Investissements d'Avenir» launched by the French Government, from la Fondation de la Recherche Médicale (Team Grant SMC202006012351 to AMLD). ANR-10-IDEX-0001-02 PSL. P.J.S received the support of Human Frontier Science Program (HFSP) RGP0032-2022 and Forschungszentrum Medizintechnik Hamburg (FMTHH, grant 04fmthh2021).

High-throughput sequencing was performed by the ICGex NGS platform of the Institut Curie supported by the grants ANR-10-EQPX-03 (Equipex) and ANR-10-INBS-09-08 (France Génomique Consortium) from the Agence Nationale de la Recherche ("Investissements d'Avenir" program), by the ITMO-Cancer Aviesan (Plan Cancer III) and by the SiRIC-Curie program (SiRIC Grant INCa-DGOS-465 and INCa-DGOS-Inserm_12554). Data management, quality control and primary analysis were performed by the Bioinformatics platform of the Institut Curie. The RNAseq data analysis was performed by GenoSplice technology (Paris, France).

We would like to thank the lab of Dr. Federica Benvenuti and the lab of Pr. Michael Sixt for providing bone marrow from WASP KO mice.

Material and methods:

Mice:

B6 : C57BL6/J, provider Charles River, catalogue : #000664.

CCR7-GFP knock in/ knock out mice: from Jackson laboratory, stock number: 027913, bred in our animal facility, original paper: Nakano H et al., 2013. CD11c-Cre mice: bred in our animal facility, original paper: Caton et al., 2007. Arpin knockout mice: were generated by CIPHE in Marsaille, IkkB knockout mice: from our collaboration with Prof.Toby Lawrence, original paper BaratinM et al., 2015. Lmna flox Vav1-Cre mice: From Manel's lab: original mice from José María González Granado, bred in our animal facility, original paper Kim Y, Zheng Y., 2013. $cPLA_2$ KO mice were generated by CIML in Marsaille. Littermates or age-mated mice were used as bone marrow donors; the breeder mice were previously backcrossed to C57BL6 for 7 generations.

Cells:

Dendritic cells were obtained following a protocol first described by (K. Inaba 1992). Both whole legs from 6 to 8 weeks old mice were flushed to obtain bone marrow. Cells are maintained in culture during 10 days in IMDM medium (Sigma-Aldrich, Darmstadt, Germany) containing 10% FBS decomplemented and filtered (Biowest, Nuaillé, France), 20 mM L-glutamine (Gibco, Waltham, Massachusetts, USA), 100 U/ml penicillin–streptomycin (Gibco, Waltham, Massachusetts, USA), 50 µM 2-mercaptoethanol (Gibco, Waltham, Massachusetts, USA), and 50 ng/ml of GM-CSF containing supernatant obtained from transfected J558 cells tested by ELISA, as previously described by (Faure-Andre 2008). At days 4 and 7 of culture, cells are detached using PBS-EDTA (5 mM) and replated at $0.5{:}10^6$ cells per milliliter of medium. At day 10, 90% of adherent cells express CD11c, an integrin family member, as well as MHC class II at medium levels which is specific to dendritic cells (33). The obtained cells can be used at day 10 or 11 as immature cells. The generation of dendritic cells from bone marrow supplemented with GM-CSF is a well-defined protocol but it promotes the differentiation of three cell types: granulocytes, macrophages, and dendritic cells (67) but they can separated during the cell culture based in their adhesion. Granulocytes are eliminated during the culture since they are non-adherent, whereas, macrophages are much more adherent than the other two cell types and stick to the bottom of the plate and thus we recover the semi-adherent dendritic cells at the last day of culture.

Dendritic cells maturation:

When using mature cells (mainly as a positive control for maturation profile of dendritic cells): Day 10 cells (which are immature when we recover them), are stimulated with 100 ng/ml of lipopolysaccharide (LPS) (Salmonella enterica serotype typhimurium; Sigma, Darmstadt, Germany) for

25 minutes and washed three times with complete medium, re-plated in fresh medium, left overnight in the incubator and then used. LPS-activated dendritic cells have higher levels of expression of the costimulatory molecules CD86 and CD40 as well as the chemokine receptor CCR7.

6-well plate confiner:

Dendritic cell confinement was performed using a 6-well plate confiner described by (Y.-J. Liu 2015) that allows the recovery of large number of cells and the simultaneous imaging of several conditions. To make the polydimethylsiloxane (PDMS, RTV615) pillars at a certain height, 12 mm glass coverslips were sonicated in methanol, washed in ethanol then plasma treated and placed on the top of a PDMS mixture on top of wafer molds that contain the pillars at the desired height. The PDMS mixture is composed of PDMS A/crosslinker B at 1/10 W/W. The height of the PDMS pillars is what determines the height of confinement of the cells between the coverslip and the bottom substrate. After adding the coverslips to the wafers, they are baked at 95° for 15 minutes, then carefully removed using isopropanol. Then they are washed again with isopropanol, dried well and plasma treated for 2 minutes. They are then incubated with non-adhesive pLL-PEG (SuSoS, PLL (20)-g [3.5]-PEG (2)) at 0.5mg/ml in 10mM HEPES pH 7.4 buffer for one hour at room temperature. The coverslips are then washed well with water to remove all the remaining PEG and incubated in cell's medium for at least 2 hours before the confinement starts. To make the confinement steps, we use a modified version of a classical 6-well plate cover; large PDMS pillars were stuck on the coverlid (these are the ones which will hold the fabricated coverslips). These large pillars will push the coverslips from the top of the lid to confine the cells. 6-well plates with glass bottom can be used in case of imaging of the cells (MatTek corporation, P06G-1.5-20-F).

Collagen gels:

Collagen gels experiments were performed based on what was described previously (68) . DCs were mixed at 4 °C with 1.6% bovine collagen type I (Advanced BioMatrix). 40 µls of the mix were deposited on a 35 mm glass-bottom dish and the drop was homogenized while covered with a 12 mm glass slide. The sample was incubated at 37 °C for 20 min to allow collagen polymerization. To generate the CCL21 gradient, 2 ml of DC medium containing 200 ng ml^{-1} of CCL21 was added to the plate. Cells were imaged overnight with a phase contrast with 10 objective and a frequency of 1 image per 2 min. Contiguous positions were stitched using the FIJI plugin Grid/collection stitching (69) to extract individual cell tracks. The mean image of the movie was subtracted from every time point and white objects in a dark background were detected. Resulting movies were processed using the FIJI plugin Filter Mean (Intensity 3) and cells were tracked using custom software (70).

Live cell imaging:

Live Time-lapse recordings were acquired with 20x (NA 0.75) dry objective, Nikon video-microscopy, for 4-6 hours at 37 °C with 5% CO2 atmosphere. Or by confocal microscope (Leica DMi8, SP8 scanning head unit) with 40x (NA 1.3) oil objective with a resolution of 1024x1024 pixels. Both microscopes were controlled by Meta Morphe software. Image analysis was performed using Imag eJ software (71) (NIH, http://rsb.info.nih.gov/ij/index.html).

For GFP quantification, imaging was done using both transmission phase and GFP. Images corresponding to each time point of interest were collected in each condition, the outline of each cell was drawn by hand on the trans images, then the mean GFP signal was calculated on the corresponding GFP image using a homemade macro; mean intensity of each cell was subtracted from the average intensity of the background, then multiplied by cell's area to calculate total GFP intensity per cell. Of note, only cells with intensity higher than the background were plotted (percentage of cells is indicated in the legends).

Constructs:

NLS_GFP: pTRIP-SFFV-EGFP-NLS (NLS-GFP hereafter) was generated introducing the SV40 NLS sequence (PKKKRKVEDP) by overlapping PCR at the C-terminal of GFP in pTRIP-SFFV that were from the lab of N.Manel (23) .

Lap2b: the plasmid was obtained by cloning LAP2b from pN2-EGFP-LAP2b (available on Addgene) into pTRIP-SFFV-EGFP that were from the lab of N.Manel using 2 restriction enzymes BsrGI and KpnI.

Lentivirus transduction:

Transduced dendritic cells were obtained by transfection of BMDCs from C57BL/6 mice were 1million cells/2ml medium were plated. At day 4, 40ml of fresh pTRIP-SFFV-GFP-NLS lentivector supernatant were loaded in Ultra-Clear Centrifuge tubes (Beckman Coulter) and ultracentrifuged at 100,000g in a SW32 rotor (Beckman coulter) for 90 minutes at 4°C and re-suspended in 400µl of in DC medium. 200µl of ultracentrifuged virus were used to infect one well of cells in presence of 8µg/ml of Protamine. Cells were then left for 48h, then washed to remove the viral particles and left in new medium till day 10 of culture.

NE fluctuation measurements:

Nuclei of live cells expressing EGFP-LAP2b (transduced with pTRIP-SFFV-EGFP-LAP2b) were recorded on a Leica DMI8 microscope, equipped with CSU-X1 Yokogawa spinning disk module. The acquisition was realized with a 63x oil objective (N.A. 1.40) and collected by the Hamamatsu Orca flash 4.0 camera.

Movies at high temporal resolution were then acquired with a 488 nm laser at 3% (exposure time 200 milliseconds) at the rate of 1 frame every 250 milliseconds for 700 timeframes using a high frame rate acquisition mode. The position of each nucleus was corrected for linear and rotational drift using the Stackreg plugin of the ImageJ/Fiji software. NE fluctuations were calculated by measuring the square root of the mean square displacement (MSD), expressed in µm. To precisely position the NE, line scans across the NE (intensities along a line of 1 pixel in width perpendicular to the NE) were made at 4 different positions per nucleus along the NE. For each point along the NE and for each time point in the movie, the point of maximum intensity was calculated on the line scan and a parabola was fitted on 5 points before and after the maxima to determine the localization of the NE with a sub-pixel resolution. For a first round of analysis, the mean position was taken as the average across all time points. Points with a displacement larger than twice the average displacement were considered outliers and removed from analysis. A new mean position was calculated from non-outliers' points and used as reference to calculate the displacement at each time point. The square root of the MSD was calculated as follows: The square root of the MSD was taken as one measure for the fluctuation of the NE. Each point along the NE contributes one measure. The values per cell were obtained by averaging the values of the corresponding kymographs. A floppy and thus less tensed, membrane is expected to fluctuate more, whereas a membrane under tension exhibits no or diminished fluctuations. Important to mention that in our hands, transduced –iDCs seemed to have bigger area than non-transduced cells.

Drugs and Reagents:

For live imaging experiments: NucBlue (Hoechst33342) from Thermo fischer (R37605) to mark the DNA. For drug treatments: AACOCF3 (selective phospholipase A_2 inhibitor, Tocris #1462-5), CK666 (selective Arp2/3 inhibitor, Tocris #3950), BI605906 (selective IKKβ inhibitor #53001).

Immunofluorescence microscopy:

The staining was done directly on the confinement plate to not affect the expression of the markers of interest. After removing the confinement led, samples were fixed directly with 4% paraformaldehyde for half an hour, permeabilized with 0.2% Triton X-100, and then incubated overnight with the primary antibodies at 4°. The next day, samples were washed with PBS and incubated with the corresponding secondary antibodies for one hour, then washed three times with PBS and mounted with fluromount solution. Imaging was done using confocal microscope (Leica DMi8, SP8 scanning head unit) with 40x (NA 1.3) oil objective with a resolution of 1024x1024 pixels. The following primary antibodies were used for the IF staining: anti-CCR7 (abcam #ab32527), anti-laminA/C (Sigma #SAB4200236), anti-$cPLA_2$ (abcam #ab58375), anti-NF-κB P65 (cell signalling #mAB 8242), Alexa Fluor-coupled Phalloidin (Invitrogen).

Calculation of the florescence intensity:

Images were acquired with SP8 confocal microscope, then Z stacks of usually 0.33 µm as a step size were made for each position, with a home-made macro, the plan of the nucleus was used to quantify the florescence intensity by making a mask on both the nucleus (taking the Dapi channel) and the cell (taking the phalloidin channel) and intensity was calculated.

Transfection and SiRNA oligonucleotides:

Bone marrow derived dendritic cells at day 7 ($3x10^6$) were transfected with 100µl of the Amaxa solution (Lonza) containing siRNA (control or target-specific) following the manufacturer's protocol. Cells were further cultured for 48-72 hours. At the day of the experiment wells were detached with medium, some cells were collected to check the efficacy of the Si step by either western blot or RT-qPCR protocols. The following SMARTpool siRNAs were used: SMARTpool: ON-TARGETplus *Pla_2g4a* siRNA (Dharmacon # L-009886-00-0010) and ON-TARGETplus Non-Targeting Control Pool (Dharmacon # D-001810-10-20).

RT-qPCR:

After removing the confinement, the lysis buffer was added directly to recover the confined cells, taking in parallel control cells that were not confined.

RNA extraction was performed using RNeasy Micro RNA kit (Qiagen), according to the manufacturer's protocol. cDNA was produced using the high capacity cDNA synthesis kit (thermo fisher), according to the manufacturer's protocol, starting from 1 µg of RNA. Quantitative PCR experiments were performed using Taqman Gene Expression Assay (Applied Biosystems) and carried out on a Lightcycler 480 (Roche) using the settings recommended by the manufacturer.

The following primers were used: Mm99999130_s1 for CCR7, Mm01284324_m1 for Pla_2g4a and Mm99999915 for GAPDH as a control. The expression of each gene of interest was assessed in immature non-confined cells. Samples were run in triplicate for each condition. Data were subsequently normalized to GAPDH values, and to the values obtained in control immature cells were used as a base unit equal to one, thus allowing for display of the data as "fold-greater" than the immature cells. The fold change was calculated by the formula $2^{-\Delta\Delta CT}$.

Flow cytometry analysis:

To characterize the expression of some surface markers on the dendritic cells after confinement we used the FACS approach. In brief, after confining the cells, the confiner was removed and cells were recovered directly by gently washing with medium. Non-confined cells activated with LPS were also

taken as controls. Cells were re-suspended in the buffer (PBS BSA 1% EDTA 2mM). After blocking with Fc antibody (BD #553142) and live/dead staining kit (Thermo # L34966) for 15 minutes, cells were stained with the desired antibodies for 20 minutes (at 37° for CCR7 staining and at 4° for the rest). Cells were then washed three times and re-suspended in the staining buffer. Flow cytometry was performed on LSRII (BD) and analyzed using FlowJo software version 10. Mean florescent values of each condition were plotted with Graphpad Prism version 8. The following antibodies were used: anti-CD80 (BD # 553769), anti-MHCII (Ozym # BLE107622), anti-CD86 (Ozyme # BLE105037), anti-CD11c (BD # 550261) with the corresponding isotypes to each antibody.

For the T-cell presentation assay: OVA peptide (Cayla #vac-isq) was added to each condition with the corresponding concentration, cells were then confined for four hours, then recovered by washing with medium and counted, T-cells which were purified from OTII mice were added to the recovered dendritic cells with a ratio of 10 to 1 respectively. Then next day, half of the medium was recovered and staining for T-cells was don. Cells were stained in 2mM EDTA, 5%FBS in PBS following the same protocol as before. Then 2 days later, the rest of the medium was recovered and sating for the T-cells was done.

Flow cytometry was performed on LSRII (BD) and analyzed using FlowJo software version 10. Percentage values were plotted with Graphpad Prism version 8. The following antibodies were used: anti-CD4 (BD # 553051), anti-CD69 (eBioscience # 48-0691-82), anti-TCR (BD # 553190).

MLR protocol:

For the mixed lymphocyte reaction (MLR) assay, allogeneic CD3+ T cells were isolated using a pan T-cell isolation kit (Miltenyi) and cultured in 96-well plates with DCs at different ratios. DCs were confined at the height of 3 µm for 4 hours then recovered and counted before adding the T-cells. Cells were cultured for 3 days, and proliferation was assessed by the addition of CFSE.

On the day of the analysis (3 days after the coculture), cells were stained in 2mM EDTA, 5%FBS in PBS following the same protocol as before and sating for the T-cells was done. Flow cytometry was performed on LSRII (BD) and analyzed using FlowJo software version 10. Percentage values were plotted with Graphpad Prism version 8.

RNA seq:

After removing the confinement, the lysis buffer was added directly to recover the confined cells, taking in parallel control cells that were not confined.

RNA extraction was performed using RNeasy Micro RNA kit (Qiagen), according to the manufacturer's protocol. The samples were checked for the quality of the extracted RNA before sending them to the NGS-sequencing platform in the institute CurieRNA sequencing libraries were prepared from 300ng to 1µg of total RNA using the Illumina TruSeq Stranded mRNA Library preparation kit and the Illumina Stranded mRNA Prep Ligation kit which allow to perform a strand specific RNA sequencing. A first step of polyA selection using magnetic beads is done to focus sequencing on polyadenylated transcripts. After fragmentation, cDNA synthesis was performed and resulting fragments were used for dA-tailing and then ligated to the TruSeq indexed adapters (for the TruSeq kit) or RNA Index Anchors (for the mRNA Ligation kit). PCR amplification was finally achieved to create the final indexed cDNA libraries (with 13 cycles).

Individual library quantification and quality assessment was performed using Qubit fluorometric assay (Invitrogen) with dsDNA HS (High Sensitivity) Assay Kit and LabChip GX Touch using a High Sensitivity DNA chip (Perkin Elmer). Libraries were then equimolarly pooled and quantified by qPCR using the KAPA library quantification kit (Roche). Sequencing was carried out on the NovaSeq 6000 instrument from Illumina using paired-end 2 x 100 bp, to obtain around 30 million clusters (60 million raw paired-end reads) per sample.

RNA seq data analysis:

The RNAseq data analysis was performed by GenoSplice technology (Paris, France). Raw data are available at GEO under the number: GSE207653.

Analysis of sequencing data quality, reads repartition (e.g., for potential ribosomal contamination), inner distance size estimation, gene body coverage, strand-specificity of library were performed using FastQC, Picard-Tools, Samtools, and RSeQC. Reads were mapped using STAR [PMID: 23104886] on the mm39 genome assembly.

Gene expression was estimated as described previously [PMID: 34495298] using Mouse FAST DB v2021_2 annotations. Only genes expressed in at least one of the two compared conditions were analyzed further. Genes were considered as expressed if their Fragments Per Kilobase Million (fpkm) value was greater than fpkm of 98% of the intergenic regions (background). Analysis at the gene level was performed using Deseq2[PMID: 25516281]. Genes were considered differentially expressed for fold-changes ≥1.5 and p-values ≤0.05. Pathway analyses and transcription factor network analysis were performed using WebGestalt 0.4.4 (72)[PMID: 31114916] merging results from upregulated and downregulated genes only, as well as all regulated genes. Pathways and networks were considered significant with p-values ≤0.05.

The graphics (heat map, pca, scatter and volcano plots) were generated using R v4.2.1 with the help of ggplot2 and ComplexHeatmaps [PMID:27207943] packages. The heat maps were created using the Z-score of Deseq2 normalized counts. The scatter plots represent the log2 fold-change of a comparison against another.

In vivo analysis of dendritic cell's subtypes:

Littermates at the age of 12-16 weeks of Arpin wild type (flox/flox cre-/-) and knockout (flox/flox cre+/-) mice were used. Both males and females.

To collect cells from the skin: 1 cm^2 part of the skin was cut with the help of a stencil, and transferred to an Eppendorf tube. 1ml of 0.25 mg/ml of liberase (Sigma #5401020001) and 0.5 mg/ml of DNAse (Sigma #10104159001) in 1 ml RPMI medium (sigma). The skin was cut using scissors and incubated 1-2 hours at 37°.

To collect cells from the lymph nodes: axial and branchial lymph nodes were removed. Then they were transferred to an Eppendorf tube containing 500µl of RPMI medium, DNAse was added at concentration of 0.5 mg/ml and collagenase at 1 mg/ml. The nodes were further cut with scissors and incubated 20 minutes at 37°.After, cells were re-suspended in PBS 0.5% BSA 2mM EDTA at 4°. Cells were filtered with cells strainer of 100 µm in a tube of 50ml. cells were centrifuged and then stained following the same protocol as explained before.

The following antibodies were used:

Anti-CCR7 (Biolegend #120114), anti-cd11c (eBioscience #25-0114-81), anti-cd326 (Biolegend #118217), anti-cd86 (BD pharmingen #553692), anti-cd11b (Biolegend #101237), anti-MHCII (eBioscience #56-5321-80), anti-cd45 (eBioscience #61-0451-82), ant-cd8a (BD bioscience #553035), anti-cd103 (eBioscience #46-1031-80). Flow cytometry was performed on LSRII (BD) and analyzed using FlowJo software version 10. Percentage values were plotted with Graphpad Prism version 8.

Statistics:

Statistical significance was calculated between two groups by Mann-Whitney test. Ordinary Mann-Whitney with multiple comparison was used to calculate statistical significance between multiple groups. Analyses were performed using GraphPad Prism 8 software.

Figure 1: **Mechanical deformation of DCs leads to CCR7 upregulation.**

(**a**) Upper panel: Schematic representation of cells in the different conditions of confinement (Created with BioRender.com). Lower panel: Representative images of live immature dendritic cells (DCs) expressing LifeAct-GFP (grey) stained with NucBlue (DNA, red) under different conditions of confinement from left to right: non-confined (NC), confined at 4 µm height, confined at 3 µm height. (**b**) Left panel: Nucleus of live cells represented in different axes. Scale bar 3 µm. Right panel: Quantification of the nucleus projected area of live cells under confinement, box plot representation where each plot is a cell. N=2, n=71 cells in NC, n=70 cells in 4 µm, n=63 cells in 3 µm, P value ordinary one-way ANOVA test p <0.0001. (**c**) Representative images of live immature DCs expressing CCR7-GFP under confinement of 4 and 3 µm heights at different time points of confinement. Top Images of transmission light (Trans) in grey and CCR7-GFP in green, lower images are GFP channel using false colors to better show differences in intensity (Min=0 Max=255). (**d**) Quantification of total GFP intensity in DCs under confinement of different conditions at different time points. Violin plot (median and quartiles) representation where each dot is a cell. Outliers were calculated using prism ROUT test (Q=1%) and represented in grey. Left panel: GFP intensity at 30 minutes of confinement: N=4, n= 348 cells in 4 µm (82% of cells), n=314 cells in 3 µm (80% of cells). Middle panel: GFP intensity at 4 hours of confinement; N=4, n= 201 cells in in 4 µm (80% of cells), n=206 cells in 3 µm (86% of cells). Right panel: GFP intensity at 6 hours of confinement: N=4 n= 215 cells in in 4 µm, n=187 cells in 3 µm. P value Mann-Whitney test ****: p <0.0001. (**e**) Left panel: Representative immunofluorescence images of immature DCs confined for 4 hours at 4 and 3 µm. After removing the confinement, CCR7 was visualized using immunostaining (in grey) and the nucleus stained with Dapi (in red). Scale bar of 5 µm. Right panel: Quantification of CCR7 mean intensity after 4 hours of confinement, box plot representation where each dot is a cell. N=2, n=74 cells in 4 µm, n=89 cells in 3 µm, P value Mann-Whitney test ****: p <0.0001. (**f**) RT-qPCR data reveals the upregulation of *Ccr7* gene upon 4 hours ofconfinement with different heights. Graph: mean with SD of *Ccr7* fold change after normalization to non-confined immature cells. Each dot represents one experiment calculated as described in the methods. N=3, P value ordinary one-way ANOVA test ****: p <0.0001. (**g**) RT-qPCR data reveals the upregulation of *Ccr7* gene upon 30 minutes of confinement with different heights. Cells were left in the incubator for 4 hours after confinement was removed, and then collected for qPCR. Mean with SD of *Ccr7* fold change after normalization to non-confined control cells. Each dot represents one experiment calculated as described in the methods. N=2, P value ordinary one-way ANOVA test **: p=0.0021 (A-C), **: p=0.0052 (B-C). (**h-i**) Chemotactic response of live immature DCs under confinement of 4 and 3 µm heights to CCL19 gradient, representative of 2 independent experiments,

n= 33 cells in 4 µm n= 43 cells in 3 µm. (**h**) Left panel: Picture of cells' trajectories under confinement in areas close to the chemokines gradient (gradient from right to left). In blue cells under 4 µm height, in orange cellsunder 3 µm height. Scale bar 100 µm. Middle panel: Representation of global steps taken by the cells under confinement with CCL19 gradient. The center of the 3 µm cells' tracks shifted towards the rightindicating an increase in their directionality towards the gradient. (**i**) Quantification of mean track speed of cells under confinement close to CCL19 gradient, box plot representation where each dot is a cell, P value Mann-Whitney test ****: p <0,0001.

Figure 2: **CCR7 upregulation in response to mechanical deformation depends on the activity of cPLA2 and the integrity of the nuclear envelope**

(**a**) Total GFP intensity quantification in DCs from CCR7-GFP mice in confinement of 3 µm height after treatment with $cPLA_2$ inhibitor AACOF3 (25 µM) or ethanol as a control. Violin plot (median and quartiles) where each dot is a cell. Outliers were calculated using prism ROUT test (Q=1%) and represented in grey. N=3, n=393 cells in control n=163 cells in AACOF3 treated, P value Mann-Whitneytest ***: p <0,0001. (**b**) Quantification of total GFP intensity in DCs from CCR7-GFP mice after knock down of $cPLA_2$ (or control) by si-RNA in confinement of 4 hours at the heights of 4 and 3 µm. Violin plot (median and quartiles) each dot is a cell, N=2, n= 25 cells in 4 µm si-ctrl (80% of cells), n=21 cells in 4 µm si-$cPLA_2$ (75% of cells), n= 16 cells in 3 µm si-ctrl (75% of cells), n=16 cells in 3 µm si-$cPLA_2$ (76%of cells), P value ANOVA test **: p= 0,0059 (A-C), P= 0,0039 (C-D). (**c**) Left panel: Representative immunofluorescence images of immature DCs from *Lmn A/C* wild type or knockout mice that were confined for 4 hours at the height of 3 µm. CCR7 was visualized using immunostaining (in grey) and thenucleus stained with Dapi (in red). Scale bar of 10 µm. Right panel: Quantification of CCR7 mean intensity signal after 4 hours of confinement, box plot representation where each dot is a cell. N=2, n=54 cells in Lmn A/C WT, n=60 cells in Lmn A/C KO, P value one-way ANOVA test ****: p <0.0001. (**d**)Left part: representative images of live immature DCs after NLS-GFP viral transduction (GFP signal in grey) to visualize nuclear envelope rupture in response to confinement at the heights of 4, 3, and 2 µm. Yellow stars were drawn to indicate the rupture and repair event. Right part: quantification of percentage of DCs displaying rupture events during the first hour of confinement with different heightsN=2. (**e**) RT-qPCR data reveals the upregulation of *Ccr7* gene upon 4 hours of confinement with different heights. Graph: mean with SD of *ccr7* fold change after normalization to non-confined control cells. Each dot represents one experiment calculated as described in the methods. N=2, P value ordinary one-way ANOVA test **: p =0.0021, ****: p <0.0001. (**f**) Left part: representative immunofluorescence images of immature DCs confined for 4 hours at the heights of 4,3, and 2 µm. $cPLA_2$ was visualized using immunostaining (in grey) and the nucleus stained with Dapi (in red). Scale bar of 10 µm. Right part: Quantification of $cPLA_2$ mean intensity, box plot representation where each dot is a cell. N=3, n=165 cells in 4 µm, n=178 cells in 3 µm, n=230 cells in 2 µm, P value Mann-Whitney test ****: p <0.0001 (**g**) Left part: representative immunofluorescence images of immature DCs from Lmn A/C WT and KO mice. Cells were confined for 4 hours at the height of 3 µm. $cPLA_2$ was visualized using immunostaining (in grey) and the nucleus stained with Dapi (in red). Scale bar of 5 µm. Right part: Quantification of $cPLA_2$ mean intensity, box plot representation where each dot is a cell. N=2, n=141 cells in WT, n=144 cells in KO, P value unpaired t-test p <0,0001. (**h**) Left part: representative immunofluorescence images of immature DCs that

were either non-confined or confined for 4 hours at the heights of 4,3, and 2 µm. Lmn A/C was visualized using immunostaining (in grey) and the nucleusstained with Dapi (in red). Scale bar of 10 µm. Right part: Quantification of Lmn A/C mean intensity. Box plot representation where each dot is a cell. N=3, n=136 cells in non-confined, n=83 cells in 4 µm,n=81 cells in 3 µm, n=126 cells in 2 µm, P value Mann-Whitney test p <0.0001. test ****: p <0.0001 (**g**) Left part: representative immunofluorescence images of immature DCs from Lmn A/C WT and KO mice. Cells were confined for 4 hours at the height of 3 µm. $cPLA_2$ was visualized using immunostaining (in grey) and the nucleus stained with Dapi (in red). Scale bar of 5 µm. Right part: Quantification of $cPLA_2$ mean intensity, box plot representation where each dot is a cell. N=2, n=141 cells in WT, n=144 cells in KO, P value unpaired t-test p <0,0001. (**h**) Left part: representative immunofluorescence images of immature DCs that were either non-confined or confined for 4 hours at the heights of 4,3, and 2 µm. Lmn A/C was visualized using immunostaining (in grey) and the nucleusstained with Dapi (in red). Scale bar of 10 µm. Right part: Quantification of Lmn A/C mean intensity. Box plot representation where each dot is a cell. N=3, n=136 cells in non-confined, n=83 cells in 4 µm,n=81 cells in 3 µm, n=126 cells in 2 µm, P value Mann-Whitney test p <0.0001.

Figure 3: **Arp2/3 tunes the $cPLA_2$ mechanical response of dendritic cells**

(**a**) *Ccr7* gene expression upon 4 hours of confinement in cells treated with CK666 (25µM) or DMSO and confined at the height of 3 µm, measured by RT-qPCR. Mean with SD of *Ccr7* fold change after normalization to non-confined control cells. Each dot represents one experiment calculated as described in the methods. N=2, P value ordinary one-way ANOVA test ****: p <0.0001, ***: p =0.0001. (**b**) Left part: representative immunofluorescence images of immature DCs treated either with CK666 (25 µM) or DMSO and confined for 4 hours at the height of 3 µm. $cPLA_2$ was visualized using immunostaining (in grey) and the nucleus stained with Dapi (in red). Scale bar of 5 µm. Right part: Quantification of $cPLA_2$ mean intensity, box plot representation where each dot is a cell. N=2, n=121 cells in control condition, n=64 cells in CK treated condition, P value Mann-Whitney test p <0.0001. (**c**) RT-qPCR data of *Ccr7* gene expression upon 4 hours of confinement in cells from $Arpin^{WT}$ or $Apin^{KO}$ mice that were confined at the heights of 4, and 3 µm. Graph represents mean with SD of *Ccr7* fold change after normalization to non-confined control cells. Each dot represents one experiment calculated as described in the methods. N=2, P values ordinary one-way ANOVA test ***: p = 0.0002, **: p= 0.0015. (**d**) Left part: representative immunofluorescence images of immature DCs from Arpin WT and KO confined for 4 hours at the heights of 4 and 3 µm. $cPLA_2$ was visualized using immunostaining (in grey) and the nucleus stained with Dapi (in red). Scale bar of 5 µm. Right part:

Quantification of $cPLA_2$ mean intensity, box plot representation where each dot is a cell. N=2, n=59 cells in WT 4 µm, n=87 cells in KO 4 µm, n=75 cells in WT 3 µm, P value ordinary one-way ANOVA test****: p <0.0001, **: P= 0.0043. (**e**) RT-qPCR data of *Ccr7* gene expression upon 4 hours of confinementin cells from $Arpin^{WT}$ or $Apin^{KO}$ that have been knocked down for $cPLA_2$ and confined at the heights of 4, and 3 µm. Graph: represents mean with SD of *Ccr7* fold change after normalization to non-confinedcontrol cells. Each dot represents one experiment calculated as described in the methods. N=2, P values ordinary one-way ANOVA test **: p = 0.0046 (B-C), **: p= 0.0080 (D-E). (**f**) Left part: representative images of live immature dendritic cells (DCs) from $Arpin^{WT}$ or $Apin^{KO}$ mice expressing LifeAct-GFP (grey) stained with NucBlue (DNA, red) under confinement of 4 and 3 µm heights, represented in different axes. Yellow stars indicating the actin cloud near the nuclear are in WT cells at 3 µm and KO cells at 4 µm. Right part: Quantification of LifeAct nuclear to cytosolic ratio calculatedas explained in supplementary figure 2. N=2, n=55 cells in WT 4 µm, n=33 cells in KO 4 µm, n=70 cells in WT 3 µm, P value ordinary one-way ANOVA test ****: p <0.0001, ***: p=0.0001. (**g**) Left part: representative immunofluorescence images of immature DCs from WASP WT and KO that were confined for 4 hours at the height of 3 µm. CCR7 was visualized using immunostaining (in grey), the nucleus stained with Dapi (in red) and actin stained with phalloidin (in green). Scale bar of 10 µm. Right part: graph: quantification of CCR7 mean intensity, box plot representation where each dot is a cell. N=2, n=70 cells in WT, n=38 cells in KO, P value unpaired t-test p <0.0001.

Figure 4: **Increased homeostatic migration in $Arpin^{KO}$ from skin to lymph nodes**

(**a**) Gating strategy to characterize dendritic cells in the skin- draining lymph nodes of $Arpin^{WT}$ and $Arpin^{KO}$ mice at steady-state conditions. Example of $Arpin^{WT}$ mouse: after gating on live cells, immune cells were CD45 high, from there gating on CD11c and MHCII was done to differentiate resident DCs (MHCII low, CD11c high) and migratory DCs (MHCII high, CD11c high). On the migratory DCs population (CD11b high, CD103 low) cells were the migratory cDCs in which (CD11b high, EPCAM low) were characteristic of the migratory DC2. On the resident DCs population (MHCII low, CD11c low) CD11b low, CD8a high DCs were characteristic of the resident DC2. (**b**) Plots of normalized number of migratory cDC2 in the skin draining lymph nodes of $Arpin^{WT}$ (*flox/flox cre-/-*) and KO (*flox/flox cre+/-*) mice, N=3 where each dot is a mouse. P value Mann-Whitney test *: p= 0,0400, ns: not-significant. (**c**) Gating strategy used to characterize dendritic cells in the skin of $Arpin^{WT}$ or $Apin^{KO}$ mice at steady-state conditions. Example of $Arpin^{WT}$ mouse: after gating on live cells, immune cells were CD45 high, MHCII high, CD11c high were DC population, among them (CD11b high, CD103 low) were the migratory DCs, from this population (CD11b high EPCAM low) were characteristic of the migratory cDC2. (**d**) Plots of

normalized number of cDC2 in the skin draining lymph nodes of Arpin^{WT} or Apin^{KO} mice, N=3 where each dot is a mouse. P value Mann-Whitney test, ns: not-significant. (**e**) Histograms of FACS analysis on the expression of CCR7 by LPS-DCs from Arpin^{WT} and Arpin^{KO} mice, representative example of 2 independent experiments. (**f**) Picture of cells' trajectories of LPS-bone marrow derived DCs from Arpin^{WT} or Apin^{KO} mice moving in collagen gels of 3ng/ml density in response to gradient of CCL19. (**g**) Analysis of directionality of these cells in the gel with and without the gradient showing no differencebetween the WT and KO of Arpin. (**h**) Analysis of cells speed in the gel with and without the gradient of CCL19 demonstrating decrease in speed in LPS activated cells from Arpin$^{WT/KO}$. N=2, n=400 cells in Arpin^{WT} without chemokine, n=485 cells in Arpin^{WT} with chemokine, n=470 cells in Arpin^{KO} without chemokine, n=468 cells in Arpin^{KO} with chemokine.

Figure 5: **A cPLA$_2$ dependent-mechanosensitive transcriptional program regulating DCs mechanical response**

(**a-e**) Data from bulk RNA-seq analysis on BMDCs from cPLA$_2^{WT}$ and cPLA$_2^{KO}$ mice. (**a**) Heat map of all the differentially expressed genes in cPLA$_2^{WT}$ and cPLA$_2^{KO}$ cells in their immature non-confined condition or immature confined at 3 µm-height. (**b**)Principal-component analysis (PCA) of the bulk RNA-Seq samples. ThePCA figure represents a two-dimensional scatterplot of the first two principal components of the RNA- Seq data. Sample groups at different confinement conditions are represented by different forms. Eachdot represents a biological replicate of an RNA-Seq sample. (**c**) Venn diagram describing the differentially expressed genes between cPLA$_2^{WT}$ and cPLA$_2^{KO}$ cells in response to confinement after normalization to the non-confined conditions using as this threshold: p value < =
0.05 and fold-change > = 1.5. (**d**) Bubble plot of some Reactom pathway enrichment analysis on the genes upregulated in cPLA$_2^{WT}$. The size of the bubble represents the number of genes in each pathway. The pathway term is displayed in Y axis, -log10 (p) is displayed in X axis. (**e**) Fragments Per Kilobase of transcript per Million mapped reads of *Ccr7* gene in the different condition of the bulk RNA-seq experiment with each color of the triplicate samples representing one condition.

Figure 6: **cPLA$_2$ mediates *Ccr7* upregulation through activity of *Ikk*β**

(**a**) Heat map of some genes moving with *Ccr7* (upregulated in cPLA$_2^{WT}$ and down regulatedin cPLA$_2^{KO}$). (**b**) RT-qPCR data of *Ccr7* gene expression upon 4 hours of confinement in cells treated with Ikkβ inhibitor BI605906 (30 µM) or with DMSO and were confined at the height of 3 µm. Graphrepresents mean with SD of *Ccr7* fold change after normalization to non-confined control cells. Each dot

represents one experiment calculated as described in the methods. N=2, P values ordinary one- way ANOVA test ****: p<0.0001, *: p= 0.0134. (**c**) RT-qPCR data of *Ccr7* gene expression upon 4 hoursof confinement in cells from *Ikbkb* ^{WT} or *Ikbkb* ^{KO} mice that were confined at the height of 3 µm. Graph: represents mean with SD of *Ccr7* fold change after normalization to non-confined control cells.Each dot represents one experiment calculated as described in the methods. N=2, P values ordinary one-way ANOVA test ****: p<0.0001, ***: p= 0.0001, ns: not-significant. (**d**) Left part: representative immunofluorescence images of immature DCs knocked down or not for $cPLA_2$ that were confined for 4 hours at the heights of 4 and 3 µm. NFκB (P65) was visualized using immunostaining (in grey) and the nucleus stained with Dapi (in red) and phalloidin (in green). Scale bar of 10 µm. Right part: Quantification of NFκB (P65) mean intensity, box plot representation where each dot is a cell. N=2, n=24 cells in si-control confined at 4 µm, n=60 cells si-$cPLA_2$ confined at 4 µm, n=60 cells si-control andsi-$cPLA_2$ confined at 3 µm, P value unpaired t-test ****: p <0.0001, ns= not-significant. (**e**) Left part: representative immunofluorescence images of immature DCs treated with Ikkβ inhibitor BI605906 (30µM) or with DMSO and confined for 4 hours at the height of 3 µm. $cPLA_2$ was visualized using immunostaining (in grey) and the nucleus stained with Dapi (in red). Scale bar of 5 µm. right part: Quantification of $cPLA_2$ mean intensity, box plot representation where each dot is a cell. N=2, n=29 cells in DMSO, n=23 cells in BI605906, P values ordinary one-way ANOVA test ns: not-significant. (**f**) Heat map of IFN-related genes that are upregulated in cPLA ^{WT} and down regulated in cPLA ^{KO}. Heatmap of innate sensing-related genes in $cPLA_2$ ^{WT} and $cPLA_2$ ^{KO} cells.

Figure 7: The $cPLA_2$-dependent mechanosensitive program shapes the immune phenotype of DCs

(**a**) Heat map of the differentially expressed genes in $cPLA_2$ ^{WT} and $cPLA_2$ ^{KO} cells treated or not with LPS. (**b**) Venn diagram describing the differentially expressed genes between 3 µm-confined and LPS DCs. (**c**) Heat map of some $cPLA_2$-related genes, $cPLA_2$ gene (*Pla2g4a*) in red. (**d**) Bubble plot of some Reactom enrichment analysis on the significantly upregulated pathways in LPS condition. (**e**) Bubble plot of some Reactom enrichment analysis on the significantly upregulated pathways in confinement condition. (**f**) Heat map of the genes in the NFκB- related pathways found in **d** (upper genes in dark orange) and in **e** (lowers genes in light orange). (**g**) FACS analysis of some immune-activating genes between DCs activated with LPS or confined at 3 µm height. Graphs showing geometric mean intensity of CD80, CD86, and MHCII. Mean with SEM, N=3 each condition was done in duplicates, each dot is the mean of one independent experiment. (**h**) Antigen presentation assays of OT-II (CD4) T-cells incubated with DCs either activated with LPS or confined at 3 µm. Left panel: percentage of $CD69^+$ positive $CD4^+$ OT-II T cells in live cells after 18 h of incubation with OVA peptide II pre-incubated with

3 µm confined or LPS-DCs. Right panel: Percentage of CFSE− $CD4^+$ OT-II T cells in live cells after 3 days of incubation with OVA peptide II pre-incubated with 3 µm confined or LPS-DCs, analyzed by flow cytometry. Graph: Mean ±SEM, N=5, P values multiple t-test, ***: $p = 0.0001$, ****: $p < 0.0001$.

Supplementary figures:

Figure S1: **GFP quantification approach**

(**a**) Quantification approach to quantify GFP intensity in each cells. (**b**) representative images of immature DCs confined for 4 hours at the height of 3 µm from C57BL/6J (WT) or GFP/GFP mice, CCR7was visualized using immunostaining (in orange) and the nucleus stained with Dapi (in cyan) scale bar10 µm.

Figure S2: $cPLA_2$ activity is not necessary for LPS-induced *Ccr7* up regulation upon confinement

(a) RT-qPCR data of $cPLA_2$ gene expression upon knock down of $cPLA_2$ with Si-RNA technique, N=3. **(b)** FACS analysis of CCR7 expression in DCs treated or not with $cPLA_2$ inhibitor AACOF3 (25 µM) after activation with LPS as described in the methods, immature DCs were taken as a control, representativeof 2 independent experiments. (**c**) RT-qPCR data of *Ccr7* gene expression in cells knocked down or notfor $cPLA_2$ and activated with LPS, data shows no difference in *Ccr7* up regulation in response to LPS in both cells types. N=2. (**d**) Left part: Representative images LAP2B-GFP transduced immature DCs underconfinement of 3 µm-height with non-confined cells as control. Right part: quantification of the meansquare displacement of the nuclear envelope of DCs under the previous conditions calculated as explained in the methods. N=3, each dot is a cell, n=34 cells in non-confined, n=51 cells in 3 µm. (**e**) RT-qPCR data of *Ccr7* gene expression in cells confined at 2 µm height and cells activated with LPS after confinement at 2 µm height, N=2. (**f**) Quantification approach of LifeAct-GFP intensity in live cells underconfinement: 1- choose Z-stack lower plan (since cells don't always touch the upper plan). 2- optical section at the surface cortex. 3-Segmentation to define cell and nuclear contour at the surface. 4- Measurement of LifeAct-GFP ratio: Actin Ratio= Nuclear surface mean actin intensity/cell surface meanactin intensity (ratio <1 => actin is mostly cortical).

Figure S3: **Bulk RNA-seq analysis shows major transcriptional changes in cells in response to confinement in a $cPLA_2$-dependent manner**

(**a**) Volcano plot representing all the differentially expressed genes in two different comparisons, in grey are the genes that have the same level of expression in both conditions, in red are the genes upregulated, and in blue are the genes down regulated. left part: illustration of the gens in LPS-DCs from $cPLA_2^{WT}$ and $cPLA_2^{KO}$ mice. Right part: illustration of the gens in confined-DCs from $cPLA_2^{WT}$ and $cPLA_2^{KO}$ mice. (**b**) Heat map of some cytokines gens in DCs in response to confinement at 3 µm-height or LPS stimulation (**c**) Upper part: heat map of some cytokines' expression by LPS or confined DCs.

Lower part: cytokine secretion analysis by luminex of the same cytokines showing their protein level of expression in the supernatant of LPS or confined DCs 48 hours after the confinement or the LPS activation. N=5 (**d**) FACS analysis on percentage of live CD11c high dendritic cells shows no difference between cells either activated with LPS or confined at 3 µm in the same presentation assay experiments showed in figure 6. Graph: mean with SEM, N=2 (**e**) MLR: mixed lymphocyte reaction analysis: dendritic cells were confined for 4 hours at 3 µm then recovered or activated with LPS and then incubated with allogeneic CD3+ T cells at different T: dendritic cell (DC) ratios for4 d. T-cell proliferation (mean + SEM) was measured by CFSE uptake. N=2.

Movie S1: Movie of BMDCs from CCR7/GFP mice under confinement.

Bone marrow derived dendritic cells from CCR7/GFP mice under confinement of 4 and 3 µm height.

Upper part is the images of cells in transmission light (in grey) and GFP signal (in green). Lower part isthe GFP signal using false colors (Physics LUT). The warmer the color the more the intensity of GFP signal. The transmission images were corrected for bleach (with the function bleach correction in ImageJ), GFP signal was smoothed using the Median filter. Time is showed in minutes (using time stamper function). Movie created with ImageJ software [67]

Movie S2: Movie of BMDCs transduced with NLS-GFP under confinement of 2 µm height.

Example of NLS-GFP expression in BMDCs under 2 µm height. The movie shows examples from 2 different positions of the same condition displaying rupture (when the GFP signal is diffused) and repair(when the signal is concentrated in the nucleus) events. The stacks were merged using the stack-mergefunction with ImageJ software. The movie is a Max Z projection of the GFP signal. Time is showed in minutes (using time stamper function).

Movie S3: Movie of live BMDCs expressing LifeAct/GFP under confinement of 4 µm height.

Example of $Arpin^{WT}$ and $Arpin^{KO}$ DCs expressing LifeAct/GFP under 4 µm height and stained with NucBlue to visualize the nucleus (DNA). Movies in Z-stack of 10 steps (step size of 0.33 µm). Upper partand lower part are $Arpin^{WT}$ and $Arpin^{KO}$ respectively. Left part is Nucleus channel, middle part is LifeAct/GFP channel, and right part is merge of both previous channels. Scale bar of 5 µm. Arrows drawn by hand to show the actin patch observed close to the nuclear area only in $Arpin^{KO}$ DC.

References

1. *Dendritic cells: specialized and regulated antigen processing machines.* **Mellman I, Steinman RM.** 2001, Cell.

2. *The priming of helper T cells.* **CA, Janeway Jr.** 1989, Semin Immunol.

3. *Dendritic cells: translating innate to adaptive immunity.* **Steinman RM, Hemmi H.** 2006, Curr Top Microbiol Immunol.

4. *Mechanisms and consequences of dendritic cell migration.* **Alvarez D, Vollmann EH, von Andrian UH.** 2008, Immunity.

5. *Dendritic cell migration in health and disease.* **Worbs T, Hammerschmidt SI, Förster R.** 2017, Nat Rev Immunol.

6. *Homeostatic NF-κB Signaling in Steady-State Migratory Dendritic Cells Regulates Immune Homeostasis and Tolerance.* **Baratin M, Foray C, Demaria O, Habbeddine M, Pollet E, Maurizio J, Verthuy C, Davanture S, Azukizawa H, Flores-Langarica A, Dalod M, Lawrence T.** 2015, Immunity.

7. *CCR7 and its Ligands: Balancing Immunity and Tolerance.* **Förster, R., Davalos-Misslitz, A. C., and Rot, A.** 2008, Nat. Rev. Immunol.

8. *Interstitial dendritic cell guidance by haptotactic chemokine gradients.* **Weber M, Hauschild R, Schwarz J, Moussion C, de Vries I, Legler DF, Luther SA, Bollenbach T, Sixt M.** 2013, Science.

9. *Dendritic Cells and the Control of Immunity.* **Banchereau, J., and Steinman, R. M.** 1998, Nature.

10. *Pathogen Recognition by the Innate Immune System.* **Himanshu Kumar, Taro Kawai & Shizuo Akira.** 2011, International Reviews of Immunology.

11. *New Insights of CCR7 Signaling in Dendritic Cell Migration and Inflammatory Diseases.* **Hong W, Yang B, He Q, Wang J, Weng Q.** 2022, Front Pharmacol.

12. *ATP promotes the fast migration of dendritic cells through the activity of pannexin 1 channels and P2X7 receptors.* **Sáez PJ, Vargas P, Shoji KF, Harcha PA, Lennon-Duménil AM, Sáez JC.** 2017, Sci Signal.

13. *Autocrine/paracrine TGF-β1 inhibits Langerhans cell migration.* **Aleh Bobr, Botond Z. Igyarto, Krystal M. Haley , Ming O. Li, Richard A. Flavell, and Daniel H. Kaplan.** 2012, PNAS.

14. *Prostaglandin E2 is a key factor for CCR7 surface expression and migration of monocyte-derived dendritic cells.* **Scandella E, Men Y, Gillessen S, Förster R, Groettrup M.** 2002, Blood.

15. *CCL19/CCL21-triggered signal transduction and migration of dendritic cells requires prostaglandin E2.* **Scandella E, Men Y, Legler DF, Gillessen S, Prikler L, Ludewig B, Groettrup M.** 2004, Bllod.

16. *Migratory dermal dendritic cells act as rapid sensors of protozoan parasites.* **Ng LG, Hsu A, Mandell MA, Roediger B, Hoeller C, Mrass P, Iparraguirre A, Cavanagh LL, Triccas JA, Beverley SM, Scott P, Weninger W.** 2008, PLoS Pathog.

17. *Luminal bacteria recruit CD103+ dendritic cells into the intestinal epithelium to sample bacterial antigens for presentation.* **Farache J, Koren I, Milo I, Gurevich I, Kim KW, Zigmond E, Furtado GC, Lira SA, Shakhar G.** 2013, Immunity.

18. *Control of Mechanotransduction by Molecular Clutch Dynamics.* **Elosegui-Artola A, Trepat X, Roca-Cusachs P.** 2018, Trends Cell Biol.

19. *Compromised nuclear envelope integrity drives TREX1-dependent DNA damage and tumor cell invasion.* **Nader GPF., Agüera-Gonzalez S, Routet F, Gratia M, Maurin M, Cancila V, Cadart C, Palamidessi A, Ramos RN, San Roman M, Gentili M, Yamada A, Williart A, Lodillinsky C, Lagoutte E, Villard C, Viovy JL, Tripodo C, Galon J, Scita G, Manel N, Chavrier P, Piel.** 2021, Cell.

20. *Emerging modes of collective cell migration induced by geometrical constraints.* **Vedula SR, Leong MC, Lai TL, Hersen P, Kabla AJ, Lim CT, Ladoux B.** 2012, Proc Natl Acad Sci U S A.

21. *Perinuclear Arp2/3-driven actin polymerization enables nuclear deformation to facilitate cell migration through complex environments.* **Thiam HR, Vargas P, Carpi N, Crespo CL, Raab M, Terriac E, King MC, Jacobelli J, Alberts AS, Stradal T, Lennon-Dumenil AM, Piel M.** 2016, Nat Commun.

22. *Editorial: Immune Cell Migration in Health and Disease.* **Renkawitz J, Donnadieu E, Moreau HD.** 2022, Front Immunol.

23. *SCRT III repairs nuclear envelope ruptures during cell migration to limit DNA damage and cell death.* **Raab M, Gentili M, de Belly H, Thiam HR, Vargas P, Jimenez AJ, Lautenschlaeger F, Voituriez R, Lennon-Duménil AM, Manel N, Piel M.** 2016, Science.

24. *The nucleus acts as a ruler tailoring cell responses to spatial constraints.* **Lomakin AJ, Cattin CJ, Cuvelier D, Alraies Z, Molina M, Nader GPF, Srivastava N, Sáez PJ, Garcia-Arcos JM, Zhitnyak IY, Bhargava A, Driscoll MK, Welf ES, Fiolka R, Petrie RJ, De Silva NS, González-Granado JM, Manel N, Lennon-Duménil AM, Müller DJ, Piel M.** 2020, Science.

25. *The Cell Nucleus Serves as a Mechanotransducer of Tissue Damage-Induced Inflammation.* **Balázs Enyedi, Mark Jelcic, Philipp Niethammer.** 2016, Cell.

26. *Intracellular calcium signals regulating cytosolic phospholipase A2 translocation to internal membranes.* **Evans JH, Spencer DM, Zweifach A, Leslie CC.** 2001, J Biol Chem.

27. *5-Lipoxygenase: mechanisms of regulation.* **Rådmark O, Samuelsson B.** 2009, J Lipid Res.

28. **Makoto Murakami, Yoshihito Nakatani, Hiroshi Kuwata, Ichiro Kudo.** Cellular components that functionally interact with signaling phospholipase A2. *Biochimica et Biophysica Acta (BBA) - Molecular and Cell Biology of Lipids.* 2000.

29. *Cytosolic phospholipase A2: physiological function and role in disease.* **C.Leslie, Christina.** 2015, Jornal of lipid research.

30. *The nucleus measures shape changes for cellular proprioception to control dynamic cell behavior.* **Venturini V, Pezzano F, Català Castro F, Häkkinen HM, Jiménez-Delgado S, Colomer-Rosell M, Marro M, Tolosa-Ramon Q, Paz-López S, Valverde MA, Weghuber J, Loza-Alvarez P, Krieg M, Wieser S, Ruprecht V.** 2020, Science.

31. *Confinement and low adhesion induce fast amoeboid migration of slow mesenchymal cells.* **Liu YJ, Le Berre M, Lautenschlaeger F, Maiuri P, Callan-Jones A, Heuzé M, Takaki T, Voituriez R, Piel M.** 2015, Cell.

32. *Actin flows mediate a universal coupling between cell speed and cell persistence.* **Paolo Maiuri, Jean-François Rupprecht, Stefan Wieser, Verena Ruprecht, Olivier Bénichou, Nicolas Carpi, Mathieu**

Coppey, Simon De Beco, Nir Gov, Carl-Philipp Heisenberg, Carolina Lage Crespo, Franziska Lautenschlaeger, Maël Le Berre, Ana-Maria Lennon-Dumen. 2015, Cell.

33. *Generation of large numbers of dendritic cells from mouse bone marrow cultures supplemented with granulocyte/macrophage colony-stimulating factor.* **Inaba K, Inaba M, Romani N, Aya H, Deguchi M, Ikehara S, Muramatsu S, Steinman RM.** 1992, J Exp Med. .

34. *Analysis of the CCR7 expression on murine bone marrow-derived and spleen dendritic cells.* **Ritter U, Wiede F, Mielenz D, Kiafard Z, Zwirner J, Körner H.** 2004, J Leukoc Biol.

35. *Migratory properties of pulmonary dendritic cells are determined by their developmental lineage.* **Nakano H, Burgents JE, Nakano K, Whitehead GS, Cheong C, Bortner CD, Cook DN.** 2013, Mucosal Immunol.

36. *Mechanisms of epithelial wound detection.* **Balázs Enyedi, Philipp Niethammer,.** 2015, Trends Cell Biol.

37. *C2 domain membrane penetration by group IVA cytosolic phospholipase A_2 induces membrane curvature changes.* **Ward KE, Ropa JP, Adu-Gyamfi E, Stahelin RV.** 2012, J Lipid Res.

38. *Nuclear deformations, from signaling to perturbation and damage.* **Nader GPF, Williart A, Piel M.** 2021, Curr Opin Cell Biol.

39. *Nuclear membrane stretch and its role in mechanotransduction.* **Enyedi B, Niethammer P.** 2017, Nucleus.

40. *Coordinated increase of nuclear tension and lamin-A with matrix stiffness outcompetes lamin-B receptor that favors soft tissue phenotypes.* **Buxboim A, Irianto J, Swift J, Athirasala A, Shin JW, Rehfeldt F, Discher DE.** 2017, Mol Biol Cell.

41. *Nuclear envelope breakdown requires overcoming the mechanical integrity of the nuclear lamina.* **Panorchan P, Schafer BW, Wirtz D, Tseng Y.** 2004, J Biol Chem.

42. *Demonstration of mechanical connections between integrins, cytoskeletal filaments, and nucleoplasm that stabilize nuclear structure.* **Andrew J. Maniotis, Christopher S. Chen, and Donald E. Ingber.** 1997, PNAS.

43. *Nuclear mechanics and mechanotransduction in health and disease.* **Isermann P, Lammerding J.** 2013, Curr Biol.

44. *The LINC complex transmits integrin-dependent tension to the nuclear lamina and represses epidermal differentiation.* **Carley E, Stewart RM, Zieman A, Jalilian I, King DE, Zubek A, Lin S, Horsley V, King MC.** 2021, Elife.

45. *Actin on and around the Nucleus.* **Davidson PM, Cadot B.** 2021, Trends Cell Biol.

46. *Inhibitory signalling to the Arp2/3 complex steers cell migration.* **Dang I, Gorelik R, Sousa-Blin C, Derivery E, Guérin C, Linkner J, Nemethova M, Dumortier JG, Giger FA, Chipysheva TA, Ermilova VD, Vacher S, Campanacci V, Herrada I, Planson AG, Fetics S, Henriot V, David V, Oguievetskaia K, Lakisic G, Pierre F, Steffen A.** 2013, Nature.

47. *Wiskott-Aldrich syndrome protein restricts cGAS/STING activation by dsDNA immune complexes.* **Piperno GM, Naseem A, Silvestrelli G, Amadio R, Caronni N, Cervantes-Luevano KE, Liv N, Klumperman J, Colliva A, Ali H, Graziano F, Benaroch P, Haecker H, Hanna RN, Benvenuti.** 2020, JCI Insight.

48. *Arpin Regulates Migration Persistence by Interacting with Both Tankyrases and the Arp2/3 Complex.* **Simanov G, Dang I, Fokin AI, Oguievetskaia K, Campanacci V, Cherfils J, Gautreau AM.** 2021, Int J Mol Sci.

49. *Impaired dendritic-cell homing in vivo in the absence of Wiskott-Aldrich syndrome protein.* **Sofia de Noronha, Samantha Hardy, Joanna Sinclair, Michael P Blundell, Jessica Strid, Oliver Schulz, Jörg Zwirner, Gareth E Jones, David R Katz, Christine Kinnon, Adrian J Thrasher.** 2005, Blood.

50. *WASp triggers mechanosensitive actin patches to facilitate immune cell migration in dense tissues.* **Gaertner F, Reis-Rodrigues P, de Vries I, Hons M, Aguilera J, Riedl M, Leithner A, Tasciyan S, Kopf A, Merrin J, Zheden V, Kaufmann WA, Hauschild R, Sixt M.** 2022, Dev.Cell.

51. *Monocytes from Wiskott-Aldrich patients display reduced chemotaxis and lack of cell polarization in response to monocyte chemoattractant protein-1 and formyl-methionyl-leucyl-phenylalanine.* **Badolato, R., Sozzani, S., Malacarne, F., Bresciani, S., Fiorini, M., Borsatti, A., Albertini, A., Mantovani, A., Ugazio, A. G., & Notarangelo, L. D.** 1998, Journal of immunology.

52. *A PGE2-MEF2A axis enables context-dependent control of inflammatory gene expression.* **Cilenti F, Barbiera G, Caronni N, Iodice D, Montaldo E, Barresi S, Lusito E, Cuzzola V, Vittoria FM, Mezzanzanica L, Miotto P, Di Lucia P, Lazarevic D, Cirillo DM, Iannacone M, Genua M, Ostuni R.** 2021, Immunity.

53. *External signals regulate continuous transcriptional states in hematopoietic stem cells.* **Fast EM, Sporrij A, Manning M, Rocha EL, Yang S, Zhou Y, Guo J, Baryawno N, Barkas N, Scadden D, Camargo F, Zon LI.** 2021, Elife.

54. *Phospholipase signalling networks in cancer.* **Park JB, Lee CS, Jang JH, Ghim J, Kim YJ, You S, Hwang D, Suh PG, Ryu SH.** 2012, Nat Rev Cancer.

55. *Macrophages, Metabolites, and Nucleosomes: Chromatin at the Intersection between Aging and Inflammation.* **Church MC, Workman JL, Suganuma T.** 2021, Int J Mol Sci.

56. *Homeostatic IL-13 in healthy skin directs dendritic cell differentiation to promote TH2 and inhibit TH17 cell polarization.* **Mayer, J.U., Hilligan, K.L., Chandler, J.S. et al.** 2021, Nat Immunol.

57. *Collagen-based cell migration models in vitro and in vivo.* **Wolf K, Alexander S, Schacht V, Coussens LM, von Andrian UH, van Rheenen J, Deryugina E, Friedl P.** 2009, Semin Cell Dev Biol.

58. *The tumor microenvironment.* **Anderson NM, Simon MC.** 2020 , Curr Biol. .

59. *A conserved dendritic-cell regulatory program limits antitumour Immunity.* **Maier B, Leader AM, Chen ST, Tung N, Chang C, LeBerichel J, Chudnovskiy A, Maskey S, Walker L, Finnigan JP, Kirkling ME, Reizis B, Ghosh S, D'Amore NR, Bhardwaj N, Rothlin CV, Wolf A, Flores R, Marron T, Rahman AH, Kenigsberg E, Brown BD, Merad M.** 2020, Nature.

60. *Blockage of Lamin-A/C loss diminishes the pro-inflammatory macrophage response.* **Johanna L. Mehl, Ashley Earle,Jan Lammerding,Musa Mhlanga, Viola Vogel, Nikhil Jain.** 2022, BioRxiv.

61. *Immunological Genome Project Consortium.* **Heng TS, et al,.** 2008, Nat Immunol.

62. *CCR7 and IRF4-dependent dendritic cells regulate lymphatic collecting vessel permeability.* **Ivanov S, Scallan JP, Kim KW, Werth K, Johnson MW, Saunders BT, Wang PL, Kuan EL, Straub AC, Ouhachi M, Weinstein EG, Williams JW, Briseño C, Colonna M, Isakson BE, Gautier EL, Förster R, Davis MJ, Zinselmeyer BH, Randolph GJ.** 2016, J Clin Invest.

63. *Locally Triggered Release of the Chemokine CCL21 Promotes Dendritic Cell Transmigration across Lymphatic Endothelia.* **Vaahtomeri K, Brown M, Hauschild R, De Vries I, Leithner AF, Mehling M, Kaufmann WA, Sixt M.** 2017, Cell Rep.

64. *CCR7 mediates human breast cancer cell invasion, migration by inducing epithelial–mesenchymal transition and suppressing apoptosis through AKT pathway.* **Xu B, Zhou M, Qiu W, Ye J, Feng Q.** 2017, Cancer Med.

65. *CCR7: Roles in cancer cell dissemination, migration and metastasis formation.* **Daniel F.Legler, EdithUetz-von Allmen, Mark A.Hauser.** 2014, The International Journal of Biochemistry & Cell Biology.

66. *Immobilized chemokine fields and soluble chemokine gradients cooperatively shape migration patterns of dendritic cells.* **Schumann K, Lämmermann T, Bruckner M, Legler DF, Polleux J, Spatz JP, Schuler G, Förster R, Lutz MB, Sorokin L, Sixt M.** 2010, Immunity.

67. *GM-CSF Mouse Bone Marrow Cultures Comprise a Heterogeneous Population of CD11c(+)MHCII(+) Macrophages and Dendritic Cells.* **Helft J, Böttcher J, Chakravarty P, Zelenay S, Huotari J, Schraml BU, Goubau D, Reis e Sousa C.** 2015, Immunity.

68. *Physical limits of cell migration: control by ECM space and nuclear deformation and tuning by proteolysis and traction force.* **Wolf K, Te Lindert M, Krause M, Alexander S, Te Riet J, Willis AL, Hoffman RM, Figdor CG, Weiss SJ, Friedl P.** 2013, J Cell Biol. .

69. *Globally optimal stitching of tiled 3D microscopic image acquisitions. .* **Preibisch S, Saalfeld S, Tomancak P.** 2009, Bioinformatics.

70. *The first World Cell Race.* **Maiuri P, Terriac E, Paul-Gilloteaux P, Vignaud T, McNally K, Onuffer J, Thorn K, Nguyen PA, Georgoulia N, Soong D, Jayo A, Beil N, Beneke J, Lim JC, Sim CP, Chu YS and WCR participants, Jiménez-Dalmaroni A, Joanny JF, Thiery JP, Erfle H, Parsons M, Mitchiso.** 2012, Curr Biol. .

71. *Image Processing with ImageJ.* **Abramoff, M.D., Magalhaes, P.J., Ram, S.J.** 2004, Biophotonics International, pp. 36-42.

72. *WebGestalt 2019: gene set analysis toolkit with revamped UIs and APIs.* **Liao Y, Wang J, Jaehnig EJ, Shi Z, Zhang B.** 2019, Nucleic Acids Res.

73. *CCR7 essentially contributes to the homing of plasmacytoid dendritic cells to lymph nodes under steady-state as well as inflammatory conditions.* **Seth S, Oberdörfer L, Hyde R, Hoff K, Thies V, Worbs T, Schmitz S, Förster R.** 2011, J Immunol.

74. **Rabin, Ronald L.** CC, C, and CX3C Chemokines. *Encyclopedia of Hormones.* s.l. : Elsevier Science Ltd., 2003.

75. *Immobilized chemokine fields and soluble chemokine gradients cooperatively shape migration patterns of dendritic cells.* **Schumann K, Lämmermann T, Bruckner M, Legler DF, Polleux J, Spatz JP, Schuler G, Förster R, Lutz MB, Sorokin L, Sixt M.** 2010, Immunity.

76. *CCR7: roles in cancer cell dissemination, migration and metastasis formation.* **Legler DF, Uetz-von Allmen E, Hauser MA.** 2014, Int J Biochem Cell Biol.

77. *High Expression of CCR7 Predicts Lymph Node Metastasis and Good Prognosis in Triple Negative Breast Cancer.* **Li X, Sun S, Li N, Gao J, Yu J, Zhao J, Li M, Zhao Z:.** 2017, Cell Physiol Biochem.

78. *Expression of the C-C Chemokine Receptor 7 Mediates Metastasis of Breast Cancer to the Lymph Nodes in Mice.* **Heather D. Cunningham, Laura A. Shannon, Psachal A. Calloway, Brian C. Fassold, Irene Dunwiddie, George Vielhauer, Ming Zhang, Charlotte M. Vines.** 2010, Translational Oncology.

79. *Nuclear deformations, from signaling to perturbation and damage.* **Nader GPF, Williart A, Piel M.** 2021, Curr Opin Cell Biol.

80. *Forcing Entry into the Nucleus.* **Lomakin A, Nader G, Piel M.** 2017, Dev Cell.

81. *New Insights of CCR7 Signaling in Dendritic Cell Migration and Inflammatory Diseases.* **Hong W, Yang B, He Q, Wang J, Weng Q.** 2022, Front Pharmacol.

82. *CXCR4 and CCR7: Two Eligible Targets in Targeted Cancer Therapy.* **Mishan, M. A., Ahmadiankia, N., and Bahrami, A. R.** 2016, Cell Biol. Int.

83. *Biased and G Protein-independent Signaling of Chemokine Receptors.* **Steen, A., Larsen, O., Thiele, S., and Rosenkilde, M. M.** 2014, Front. Immunol.

84. *Leukocyte Migration and Deformation in Collagen Gels and Microfabricated Constrictions.* **Sáez PJ, Barbier L, Attia R, Thiam HR, Piel M, Vargas P.** 2018, Methods Mol Biol.

85. *Johanna L. Mehl, Ashley Earle, Jan Lammerding, Musa Mhlanga, Viola Vogel, Nikhil Jain.* **response, Blockage of Lamin-A/C loss diminishes the pro-inflammatory macrophage.** BioRxiv.

86. *Innate control of actin nucleation determines two distinct migration behaviours in dendritic cells.* **Vargas P, Maiuri P, Bretou M, Sáez PJ, Pierobon P, Maurin M, Chabaud M, Lankar D, Obino D, Terriac E, Raab M, Thiam HR, Brocker T, Kitchen-Goosen SM, Alberts AS, Sunareni P, Xia S, Li R, Voituriez R, Piel M, Lennon-Duménil AM.** 2016, Nat Cell Biol.

87. *Lysosome signaling controls the migration of dendritic cells.* **Bretou M, Sáez PJ, Sanséau D, Maurin M, Lankar D, Chabaud M, Spampanato C, Malbec O, Barbier L, Muallem S, Maiuri P, Ballabio A, Helft J, Piel M, Vargas P, Lennon-Duménil AM.** 2017, Sci Immunol.

Figure 1

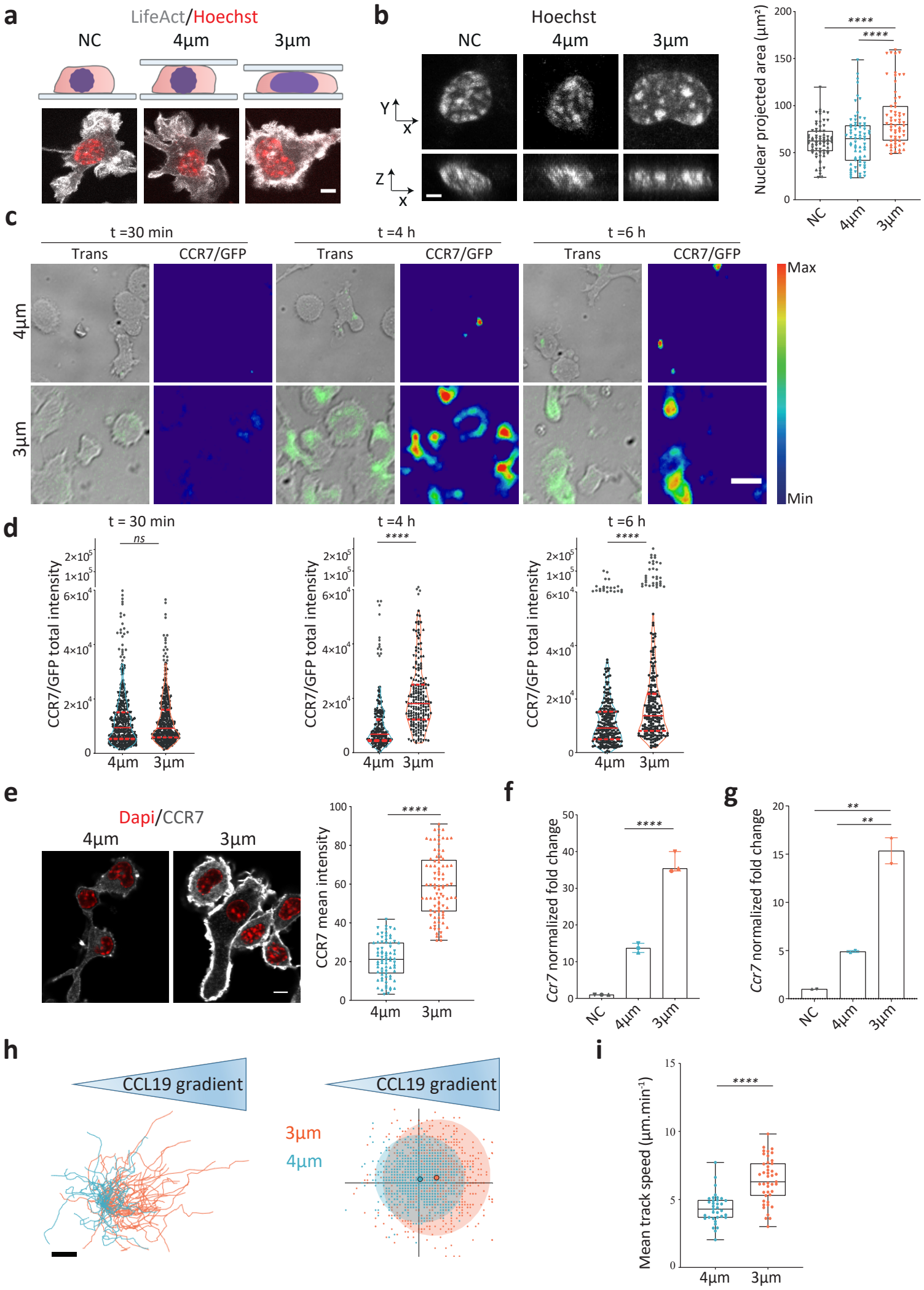
a
LifeAct/Hoechst
NC
4µm
3µm
b
Hoechst
NC
4µm
3µm
Y
X
Z
X
Nuclear projected area (µm²)
200
150
100
50
0
****
****
NC
4µm
3µm
c
t =30 min
t =4 h
t =6 h
Trans
CCR7/GFP
Trans
CCR7/GFP
Trans
CCR7/GFP
4µm
3µm
Max
Min
d
t = 30 min
t =4 h
t =6 h
ns
****
****
CCR7/GFP total intensity
2×10^5
1×10^5
6×10^4
4×10^4
2×10^4
0
4µm
3µm
e
Dapi/CCR7
4µm
3µm
CCR7 mean intensity
100
80
60
40
20
0
****
4µm
3µm
f
Ccr7 normalized fold change
50
40
30
20
10
0
****
NC
4µm
3µm
g
Ccr7 normalized fold change
20
15
10
5
0
**
**
NC
4µm
3µm
h
CCL19 gradient
CCL19 gradient
3µm
4µm
i
Mean track speed (µm.min⁻¹)
15
10
5
0
****
4µm
3µm

Figure 2

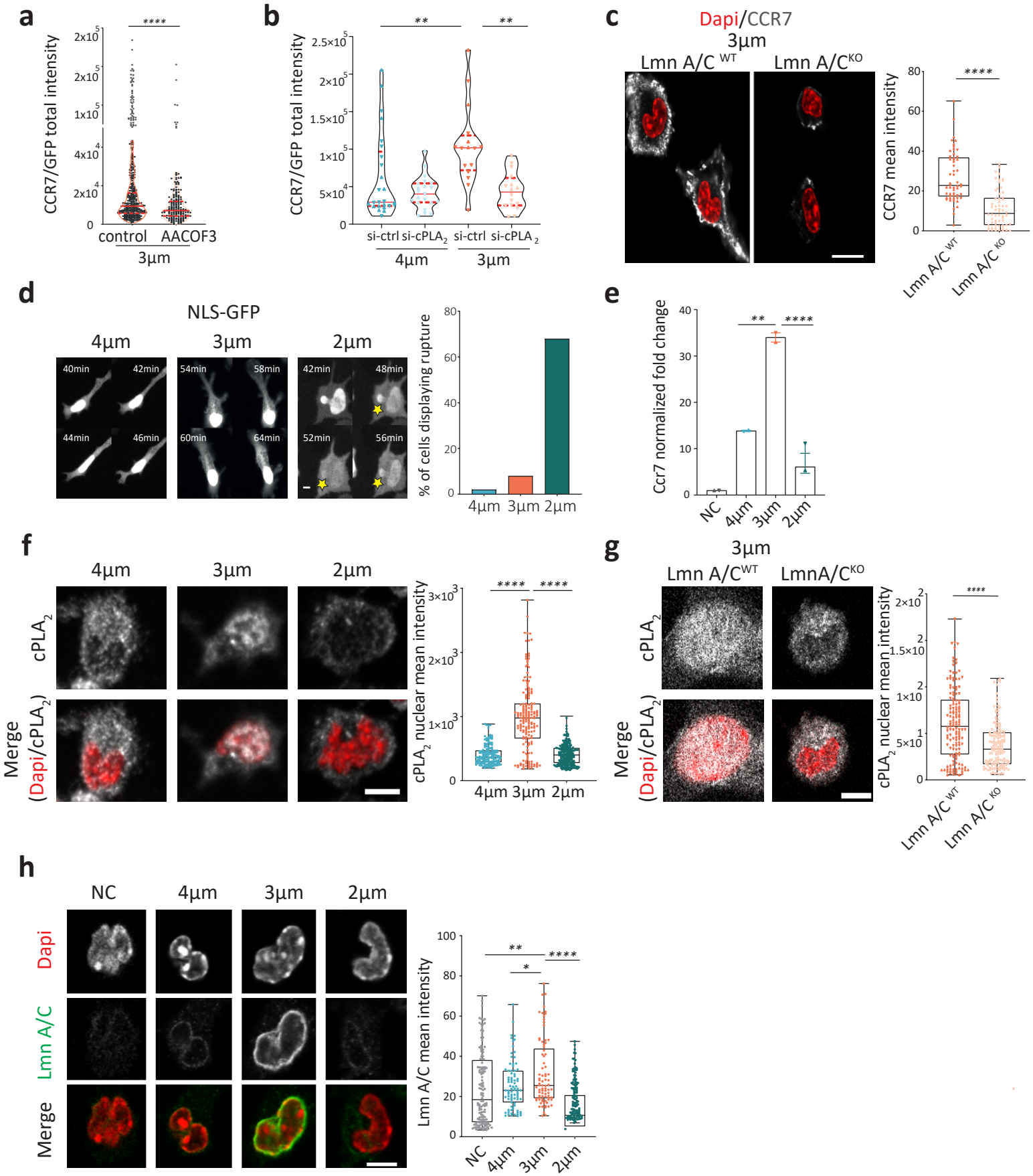
a
CCR7/GFP total intensity
control
AACOF3
3µm
b
CCR7/GFP total intensity
si-ctrl
si-cPLA2
4µm
3µm
c
Dapi/CCR7
3µm
Lmn A/C WT
Lmn A/C KO
CCR7 mean intensity
d
NLS-GFP
4µm
3µm
2µm
% of cells displaying rupture
e
Ccr7 normalized fold change
NC
f
cPLA2
Merge (Dapi/cPLA2)
cPLA2 nuclear mean intensity
g
LmnA/C KO
h
Dapi
Lmn A/C
Merge
Lmn A/C mean intensity

Figure 3

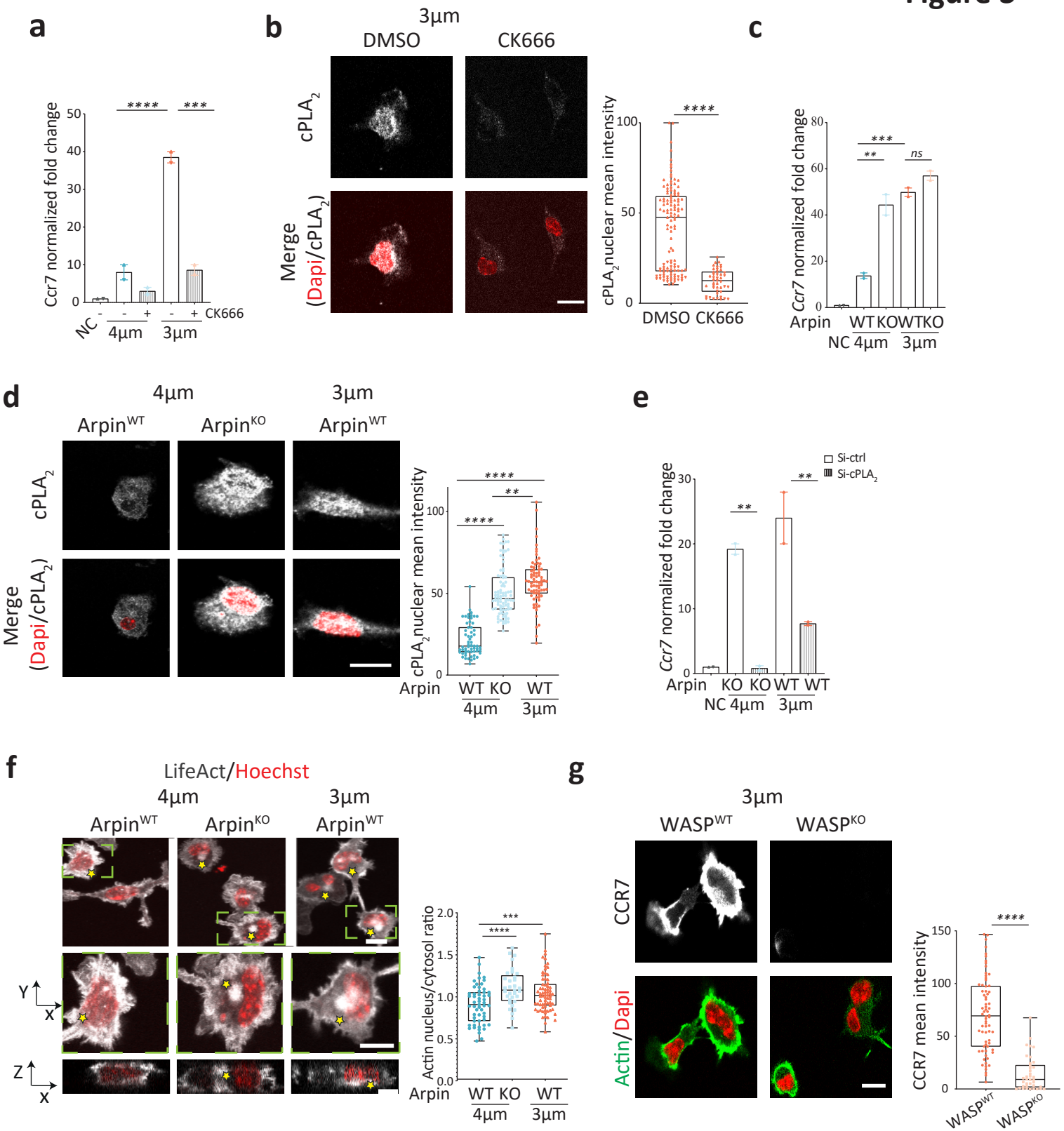
a
Ccr7 normalized fold change
****
***
NC
4µm
3µm
CK666
b
3µm
DMSO
CK666
cPLA2
Merge (Dapi/cPLA2)
cPLA2 nuclear mean intensity
****
DMSO CK666
c
Ccr7 normalized fold change
***
**
ns
Arpin
WT KO WT KO
NC 4µm 3µm
d
4µm
3µm
ArpinWT
ArpinKO
ArpinWT
cPLA2
Merge (Dapi/cPLA2)
cPLA2 nuclear mean intensity
****
**
Arpin
WT KO WT
4µm 3µm
e
Si-ctrl
Si-cPLA2
Ccr7 normalized fold change
**
Arpin
KO KO WT WT
NC 4µm 3µm
f
LifeAct/Hoechst
4µm
3µm
ArpinWT
ArpinKO
ArpinWT
Y
X
Z
X
Actin nucleus/cytosol ratio
***
****
Arpin
WT KO WT
4µm 3µm
g
3µm
WASPWT
WASPKO
CCR7
Actin/Dapi
CCR7 mean intensity
****
WASPWT
WASPKO

Figure 4

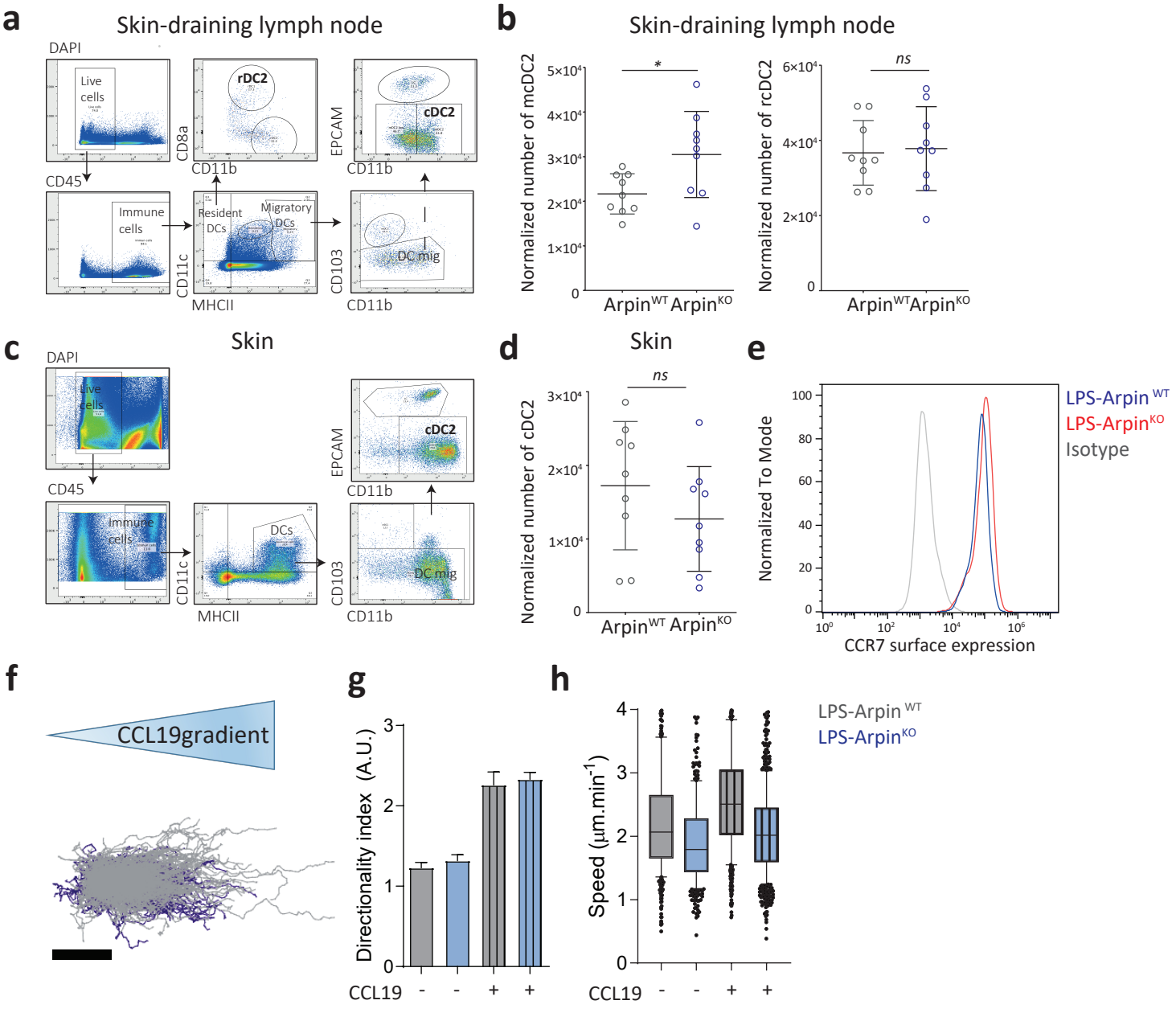
a
Skin-draining lymph node
DAPI
Live cells
CD45
Immune cells
CD8a
rDC2
CD11b
Resident DCs
Migratory DCs
CD11c
MHCII
EPCAM
cDC2
CD103
DC mig
b
Skin-draining lymph node
Normalized number of mcDC2
Normalized number of rcDC2
*
ns
ArpinWT ArpinKO
c
Skin
d
Skin
Normalized number of cDC2
e
Normalized To Mode
CCR7 surface expression
LPS-Arpin WT
LPS-ArpinKO
Isotype
f
CCL19gradient
g
Directionality index (A.U.)
CCL19
h
Speed (µm.min-1)
LPS-Arpin WT
LPS-ArpinKO

Figure 5

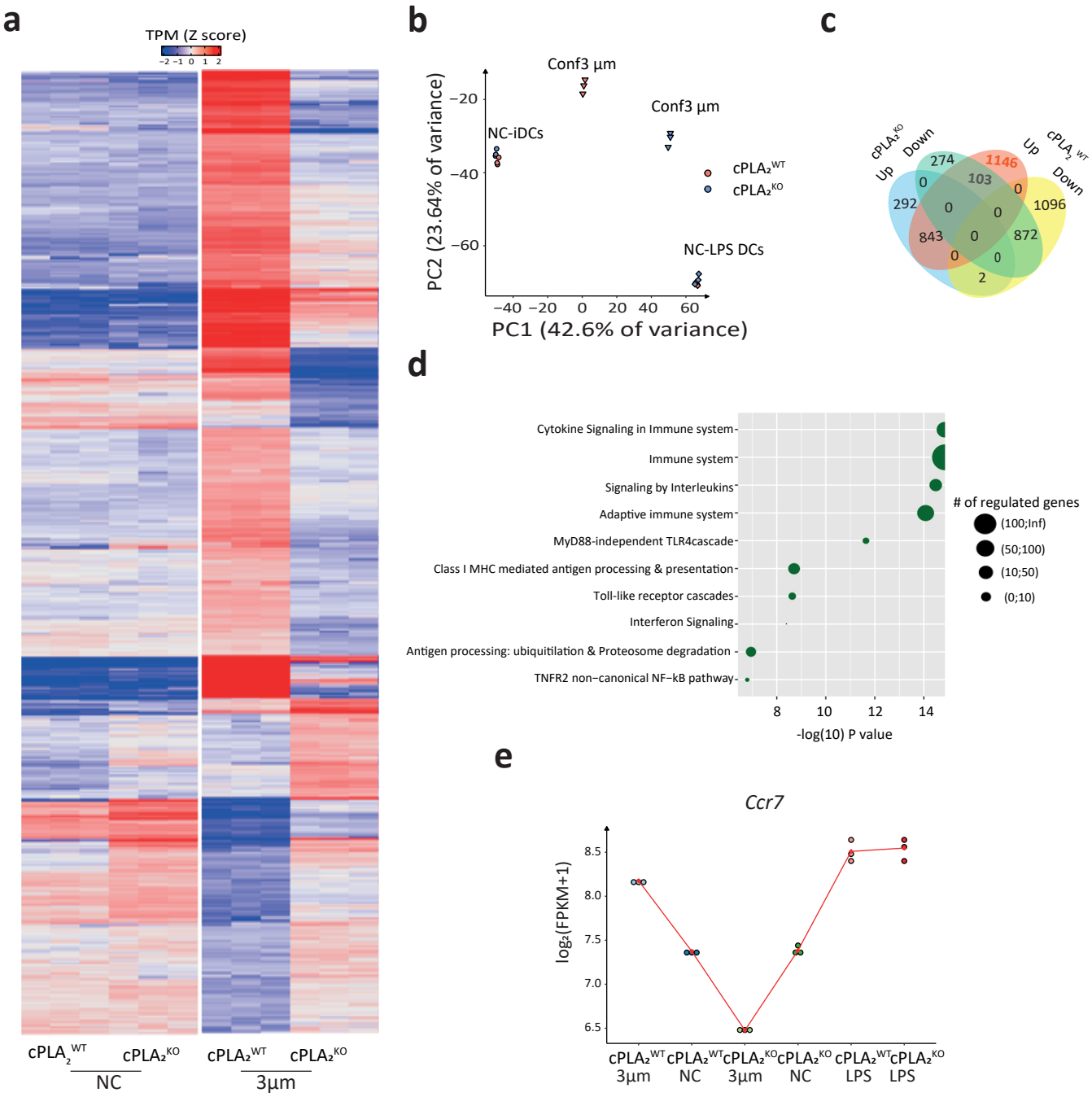
a
TPM (Z score)
−2 −1 0 1 2
cPLA2WT
cPLA2KO
cPLA2WT
cPLA2KO
NC
3µm
b
Conf3 µm
Conf3 µm
NC-iDCs
NC-LPS DCs
cPLA2WT
cPLA2KO
PC2 (23.64% of variance)
PC1 (42.6% of variance)
−20
−40
−60
−40 −20 0 20 40 60
c
cPLA2KO Up
cPLA2KO Down
cPLA2WT Up
cPLA2WT Down
274
1146
103
0
0
292
0
0
1096
843
0
872
0
0
2
d
Cytokine Signaling in Immune system
Immune system
Signaling by Interleukins
Adaptive immune system
MyD88-independent TLR4cascade
Class I MHC mediated antigen processing & presentation
Toll-like receptor cascades
Interferon Signaling
Antigen processing: ubiquitilation & Proteosome degradation
TNFR2 non−canonical NF−kB pathway
8 10 12 14
-log(10) P value
# of regulated genes
(100;Inf)
(50;100)
(10;50)
(0;10)
e
Ccr7
log2(FPKM+1)
8.5
8.0
7.5
7.0
6.5
cPLA2WT 3µm
cPLA2WT NC
cPLA2KO 3µm
cPLA2KO NC
cPLA2WT LPS
cPLA2KO LPS

Figure 6

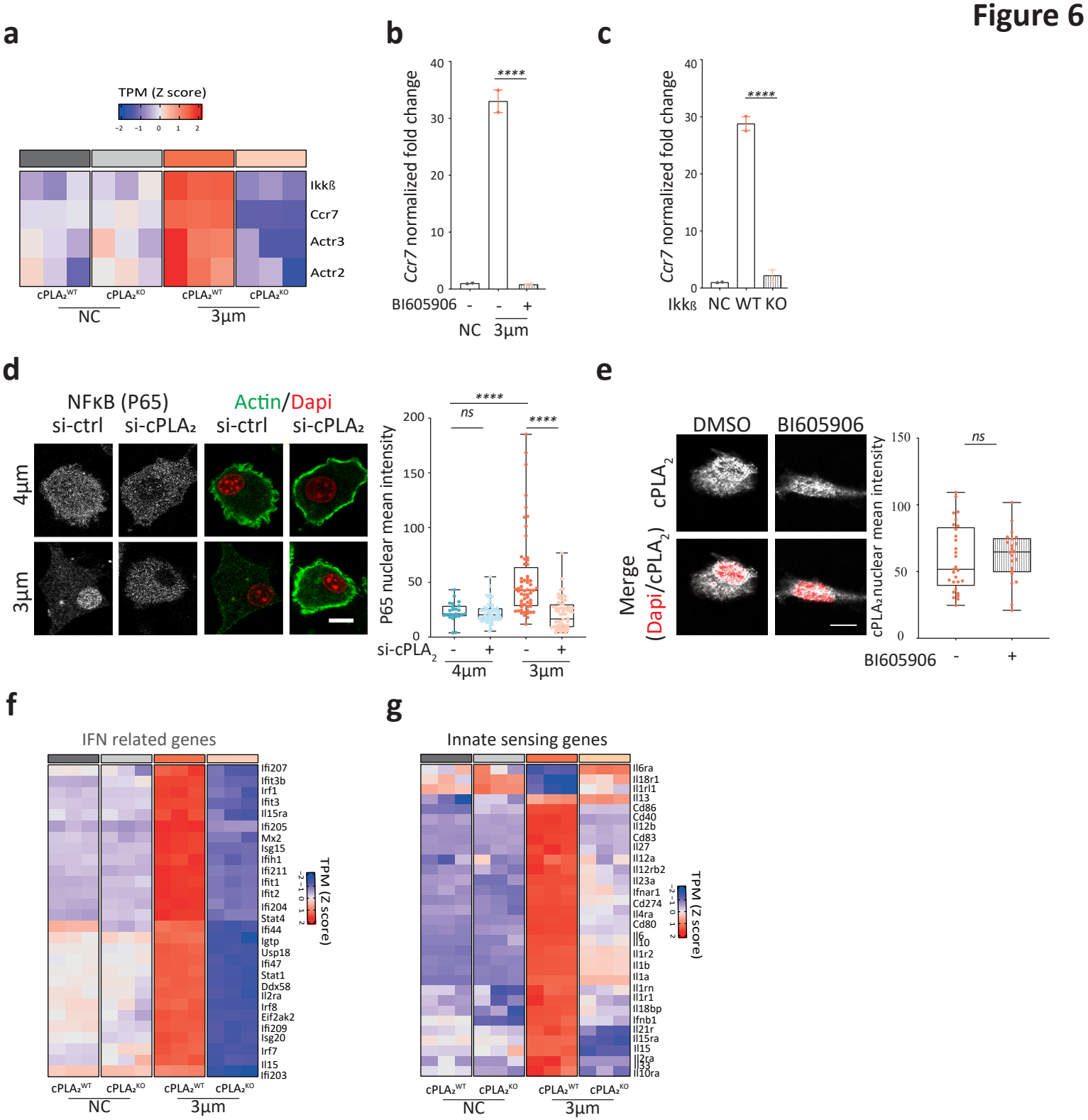
a
TPM (Z score)
-2 -1 0 1 2
Ikkß
Ccr7
Actr3
Actr2
cPLA₂WT cPLA₂KO cPLA₂WT cPLA₂KO
NC
3µm
b
Ccr7 normalized fold change
****
BI605906 - - +
NC 3µm
c
Ccr7 normalized fold change
****
Ikkß NC WT KO
d
NFκB (P65)
Actin/Dapi
si-ctrl si-cPLA₂ si-ctrl si-cPLA₂
4µm
3µm
P65 nuclear mean intensity
ns
****
****
si-cPLA2 - + - +
4µm 3µm
e
DMSO BI605906
cPLA2
Merge (Dapi/cPLA2)
cPLA₂ nuclear mean intensity
ns
BI605906 - +
f
IFN related genes
Ifi207
Ifit3b
Irf1
Ifit3
Il15ra
Ifi205
Mx2
Isg15
Ifih1
Ifi211
Ifit1
Ifit2
Ifi204
Stat4
Ifi44
Igtp
Usp18
Ifi47
Stat1
Ddx58
Il2ra
Irf8
Eif2ak2
Ifi209
Isg20
Irf7
Il15
Ifi203
TPM (Z score)
cPLA₂WT cPLA₂KO cPLA₂WT cPLA₂KO
NC
3µm
g
Innate sensing genes
Il6ra
Il18r1
Il1rl1
Il13
Cd86
Cd40
Il12b
Cd83
Il27
Il12a
Il12rb2
Il23a
Ifnar1
Cd274
Il4ra
Cd80
Il6
Il10
Il1r2
Il1b
Il1a
Il1rn
Il1r1
Il18bp
Ifnb1
Il21r
Il15ra
Il15
Il2ra
Il33
Il10ra
TPM (Z score)
cPLA₂WT cPLA₂KO cPLA₂WT cPLA₂KO
NC
3µm

Figure 7

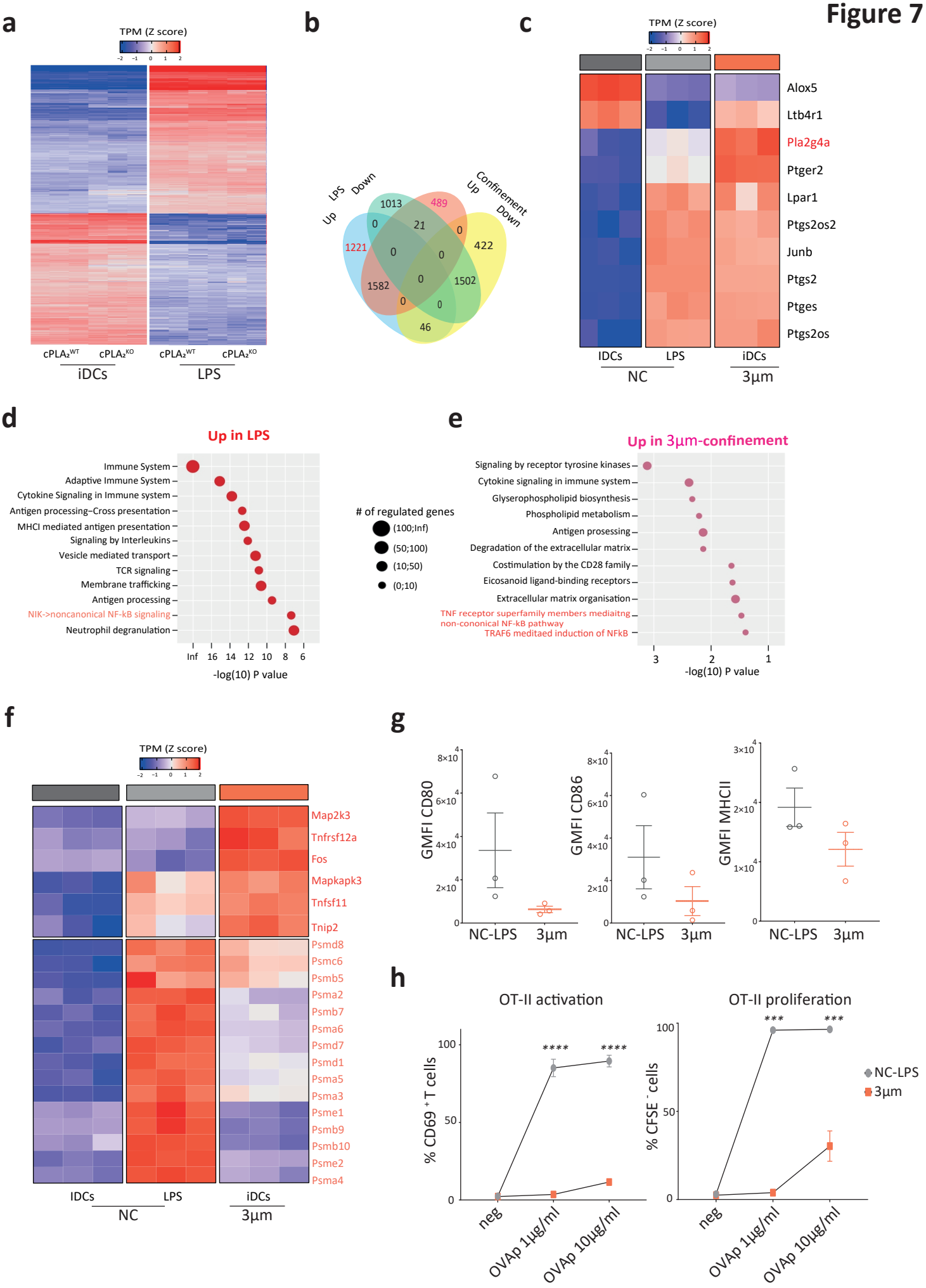
a
TPM (Z score)
cPLA2WT
cPLA2KO
cPLA2WT
cPLA2KO
iDCs
LPS
b
LPS Up
LPS Down
Confinement Up
Confinement Down
1221
1013
489
422
0
21
0
0
0
1582
0
1502
0
0
46
c
TPM (Z score)
Alox5
Ltb4r1
Pla2g4a
Ptger2
Lpar1
Ptgs2os2
Junb
Ptgs2
Ptges
Ptgs2os
IDCs
LPS
iDCs
NC
3µm
d
Up in LPS
Immune System
Adaptive Immune System
Cytokine Signaling in Immune system
Antigen processing–Cross presentation
MHCI mediated antigen presentation
Signaling by Interleukins
Vesicle mediated transport
TCR signaling
Membrane trafficking
Antigen processing
NIK->noncanonical NF-kB signaling
Neutrophil degranulation
Inf 16 14 12 10 8 6
-log(10) P value
# of regulated genes
(100;Inf)
(50;100)
(10;50)
(0;10)
e
Up in 3µm-confinement
Signaling by receptor tyrosine kinases
Cytokine signaling in immune system
Glyserophospholipid biosynthesis
Phospholipid metabolism
Antigen prosessing
Degradation of the extracellular matrix
Costimulation by the CD28 family
Eicosanoid ligand-binding receptors
Extracellular matrix organisation
TNF receptor superfamily members mediaitng non-cononical NF-kB pathway
TRAF6 meditaed induction of NFkB
3 2 1
-log(10) P value
f
TPM (Z score)
Map2k3
Tnfrsf12a
Fos
Mapkapk3
Tnfsf11
Tnip2
Psmd8
Psmc6
Psmb5
Psma2
Psmb7
Psma6
Psmd7
Psmd1
Psma5
Psma3
Psme1
Psmb9
Psmb10
Psme2
Psma4
IDCs
LPS
iDCs
NC
3µm
g
GMFI CD80
GMFI CD86
GMFI MHCII
NC-LPS
3µm
h
OT-II activation
OT-II proliferation
% CD69+ T cells
% CFSE- cells
****
***
NC-LPS
3µm
neg
OVAp 1µg/ml
OVAp 10µg/ml

Figure S1

a

1. Choose the time point of interest
2. Draw each cell's outline and add to ROI manager
3. Measure the mean GFP intensity per cell
4. Total GFP Intensity = (mean intensity - median of the background)* cell area

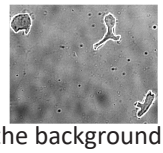

b

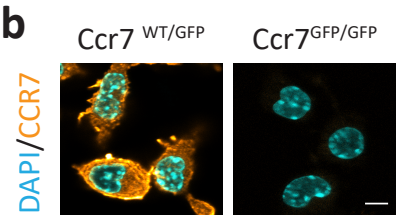

Figure S2

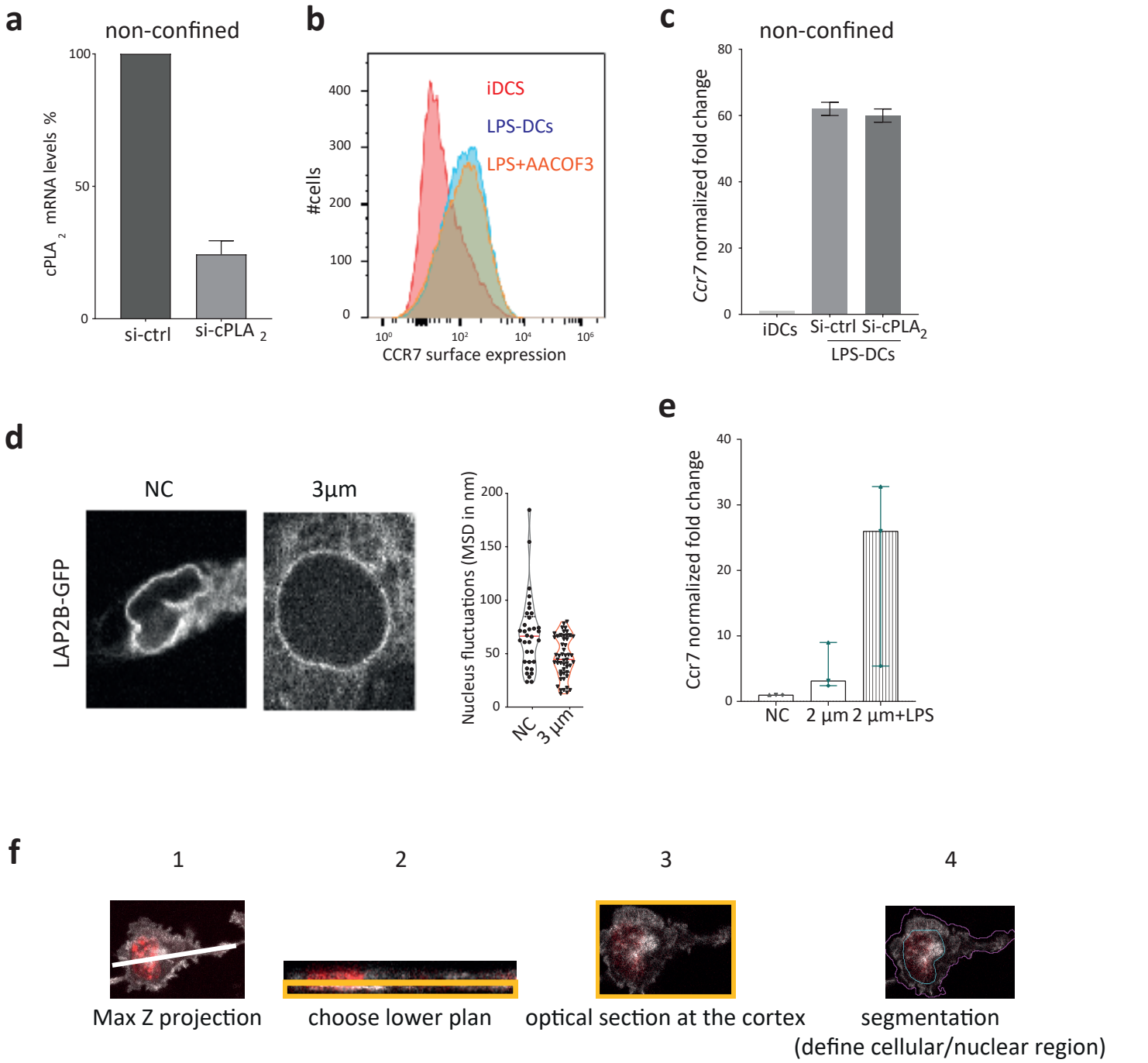
a
non-confined
cPLA2 mRNA levels %
100
50
0
si-ctrl
si-cPLA 2
b
#cells
400
300
200
100
0
iDCS
LPS-DCs
LPS+AACOF3
10⁰
10²
10⁴
10⁶
CCR7 surface expression
c
non-confined
Ccr7 normalized fold change
80
60
40
20
0
iDCs
Si-ctrl
Si-cPLA2
LPS-DCs
d
NC
3µm
LAP2B-GFP
Nucleus fluctuations (MSD in nm)
200
150
100
50
0
NC
3 µm
e
Ccr7 normalized fold change
40
30
20
10
0
NC
2 µm
2 µm+LPS
f
1
2
3
4
Max Z projection
choose lower plan
optical section at the cortex
segmentation
(define cellular/nuclear region)

Figure S3

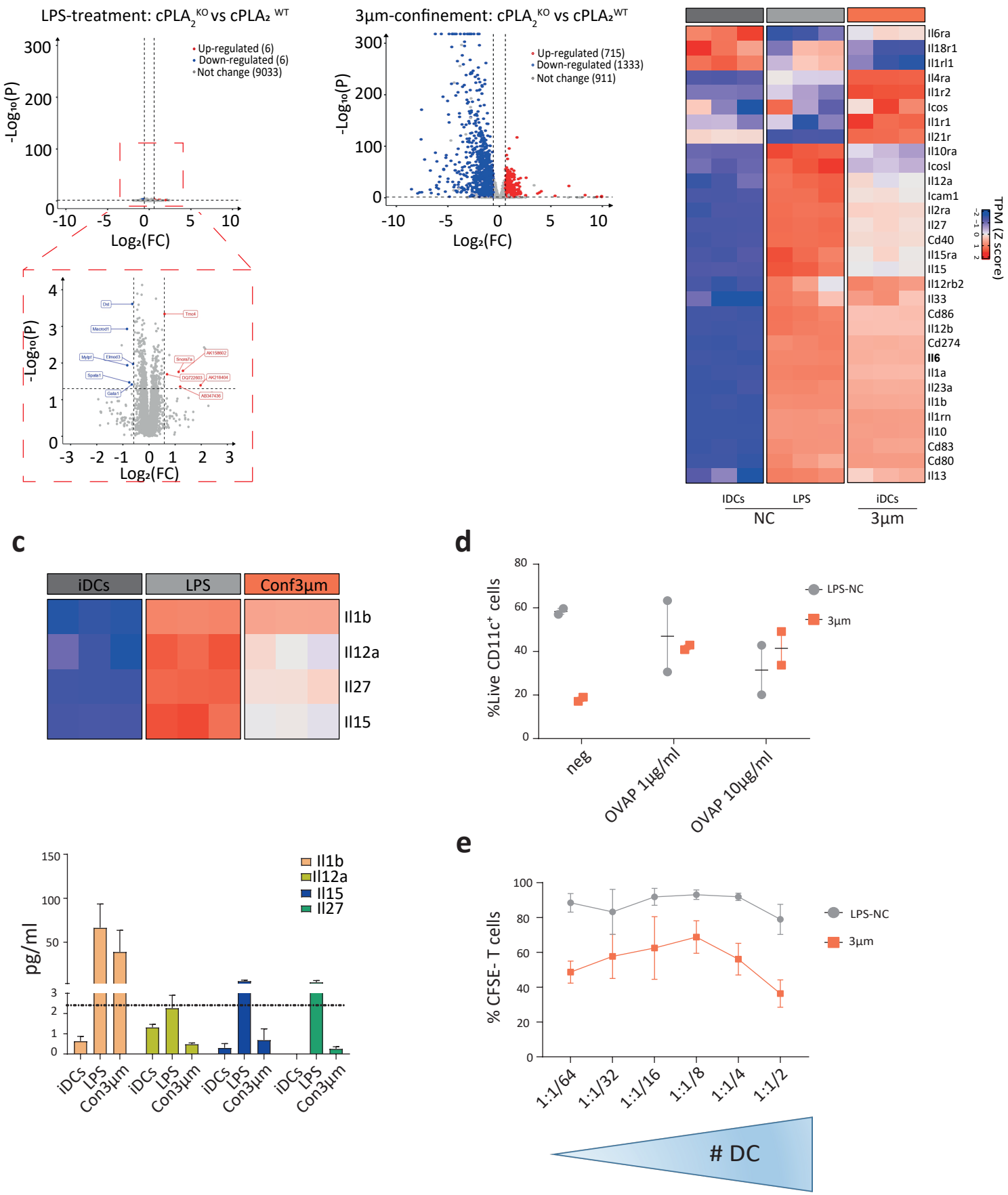
a
LPS-treatment: cPLA2KO vs cPLA2 WT
Up-regulated (6)
Down-regulated (6)
Not change (9033)
-Log10(P)
Log2(FC)
3µm-confinement: cPLA2KO vs cPLA2WT
Up-regulated (715)
Down-regulated (1333)
Not change (911)
b
Il6ra
Il18r1
Il1rl1
Il4ra
Il1r2
Icos
Il1r1
Il21r
Il10ra
Icosl
Il12a
Icam1
Il2ra
Il27
Cd40
Il15ra
Il15
Il12rb2
Il33
Cd86
Il12b
Cd274
Il6
Il1a
Il23a
Il1b
Il1rn
Il10
Cd83
Cd80
Il13
TPM (Z score)
IDCs
LPS
iDCs
NC
3µm
c
iDCs
LPS
Conf3µm
Il1b
Il12a
Il27
Il15
pg/ml
Il1b
Il12a
Il15
Il27
iDCs
LPS
Con3µm
d
%Live CD11c+ cells
LPS-NC
3µm
neg
OVAP 1µg/ml
OVAP 10µg/ml
e
% CFSE- T cells
LPS-NC
3µm
1:1/64
1:1/32
1:1/16
1:1/8
1:1/4
1:1/2
DC